NASA CONTRACTOR
REPOR,

NASA CR-143964

EXTENSION OF FOUR-DIMENSIONAL ATMOSPHERIC MODELS

By Mary Grace Fowler, Anthony S. Lisa and Shu Lin Tung
Environmental Research and Technology, Inc.
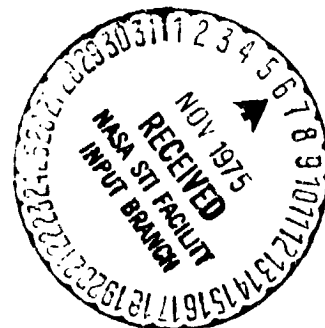Concord, Massachusetts

October 1975

Final Report

Prepared for

NASA- GEORGE C. MARSHALL SPACE FLIGHT CENTER
Marshall Space Flight Center, Alabama 35812

1. Report No. NASA CR-143964	2. Government Accession No.	3. Recipient's Catalog No.
4. Title and Subtitle EXTENSION OF FOUR-DIMENSIONAL ATMOSPHERIC MODELS		5. Report Date October 1975
		6. Performing Organization Code
7. Author(s) Mary Grace Fowler, Anthony S. Lisa and Shu-Lin Tung		8. Performing Organization Report No. P-830F
9. Performing Organization Name and Address Environmental Research & Technology, Inc. 696 Virginia Road, Concord, Mass. 01742		10. Work Unit No.
		11. Contract or Grant No. NAS8-30273
12. Sponsoring Agency Name and Address NASA Washington, D.C.		13. Type of Report and Period Covered Final Report, March 1974 - April 1975
		14. Sponsoring Agency Code

15. Supplementary Notes

Prepared under the technical direction of the Aerospace Environment Division, NASA - Marshall Space Flight Center

16. Abstract

This is the final report in a study designed to further examine the applicability of NASA MSFC global cloud statistics, and to extend the 4-D atmospheric model upwards to 52 km while incorporating wind statistics.

Comparison of satellite and surface observed cloud cover amounts for LANDSAT-1 cameras showed excellent agreement for the 1/2° field of view. Satellite cloud cover amounts measured in the 1/4° field of view showed approximately 5% less coverage than that seen from the surface. Cloud shadows added approximately 5% to the total surface obscuration for a large set of sun elevation angles and cloud amounts, but effects were much greater for elevation angles of less than 20° and cloud cover amounts between 20 and 50%.

Monthly means and variances of pressure, temperature, density and winds were derived at 2 km levels from 26 km to 52 km at 5° latitude-longitude intersections from the Greenwich Meridian west to 160° E and from the equator to the North Pole. These statistics showed good agreement with other empirical models while providing more detailed information on spatial and temporal variabilities.

Finally, monthly means and variances were derived for the east-west and north-south wind components at 1 km levels from the surface to 25 km. These winds are for the same 3,490 grid points used in the original 4-D global atmospheric model and supplement the thermodynamic parameters given there. Thus, all basic meteorological parameters are now included in the 4-D model.

17. Key Words (Suggested by Author(s)) 4-D atmospheric model global wind statistics empirical stratospheric model satellite cloud cover observations	18. Distribution Statement Unclassified - Unlimited Charles A. Lundquist	
19. Security Classif. (of this report) Unclassified	20. Security Classif. (of this page) Unclassified	21. No. of Pages 73	22. Price*

TABLE OF CONTENTS

LIST OF ILLUSTRATIONS

Page

LIST OF ILLUSTRATIONS (Continued)

LIST OF ILLUSTRATIONS (Continued)

LIST OF TABLES

1. INTRODUCTION

Remote sensing experiments require a thorough understanding of the earth's atmosphere. Clouds often obscure the earth's surface in the visible bands and significantly attenuate or totally absorb signals at microwave and infrared wavelengths. Thus accurate prediction of the occurrence, thickness and extent of clouds is necessary for the planning of earth viewing missions such as LANDSAT (formerly ERTS). Water vapor also plays a key role in the absorption of radiometric signals, an effect which is not only dependent upon the total amount of vapor but also upon the vertical distribution and temperature of this water vapor.

To meet these needs, the Aerospace Environment Division at the Marshall Space Flig Center sponsored the development of a global data bank of cloud statistics and a four-dimensional atmospheric model. The cloud data bank was developed by Sherr et al (1968) and modified by subsequent studies. It consists of thirty cloud regions with frequency of occurrence of cloud cover, cloud type and number of cloud layers given at three hour intervals for each month. The 4-D atmospheric model (Spiegler and Greaves, 1971; Spiegler and Fowler, 1972) provides means and variances of pressure, temperature, water vapor and density at 1 km levels from the surface to 25 km at 3490 points covering the globe. Both models are associated with a large set of computer programs designed to simulate meteorological conditions for any location above the earth. These data banks and models have been used to simulate many satellite missions (e.g., Chang and Fowler, 1973; Fowler, et al, 1974) and have proved to be of great value in planning and analyzing radiometric experiments.

The purpose of the current study was to expand further the atmospheric model to provide information for space vehicle design and to permit simulation of vehicle re-entry trajectories. In addition, the high resolution cameras carried by LANDSAT 1 required a revised analysis of the relationship between satellite and surface observed cloud cover to update the cloud simulation programs. Thus this report covers three broad areas designed to improve the existing models.

1

- An investigation of the relationship between satellite and surface observed cloud cover using LANDSAT 1 photographs and including the effects of cloud shadows.

- The extension of the 4-D model to the altitude of 52 km providing grid point means and variances at 2 km intervals for the parame ers of pressure, temperature, density and u and v wind components.

- The addition to the initial 4-D model of means and variances of u and v wind components at 1 km levels from the surface to 25 km.

These topics, although united in the overall goal of improving the simulation of atmospheric effects, do represent separate areas of research and development. Thus in this report they will be presented separately with Section 2 discussing the findings of the cloud cover analysis, Section 3 presenting the stratospheric model, and Section 4 presenting the tropospheric wind profiles. Section 5 will then provide the general summary and conclusions with recommendations for further improvement of the models.

2. SATELLITE AND SURFACE OBSERVATIONS OF CLOUD COVER

In the simulation of earth-viewing space missions such as LANDSAT, one of the most important parameters is cloud cover. Clouds obscure the surface at visible wavelengths and significantly attenuate infrared wavelengths, so much of the success of earth observation relies on the occurrence of clear or partially clear situations. In a long series of studies (e.g., Chang and Willand, 1972) a set of global cloud statistics has been derived to provide frequency distributions of cloud cover, cloud type and number of cloud layers for 30 cloud climatological regions. These statistics, combined with a set of computer simulation models, have been used successfully to simulate the cloud conditions along suborbital tracks and to assist in planning earth observations from space.

Despite the success of the simulations based upon these statistics, the validity of this cloud model has often been questioned on the grounds that the cloud cover statistics are based on surface observations. Studies have shown (e.g., Barnes and Chang, 1968) that there can be significant differences between the amount of cloudiness observed by a satellite and that observed from the ground. These differences arise from many sources: low resolution of satellite photographs which does not permit identification of small cumulus cells, overestimation of cloud amounts by a ground observer because of the "curvature of the sky", lack of correlation in the fields of view seen by the satellite and by the ground observer, and many other factors.

These measurement differences could possibly be resolved if both space-borne and ground-based observers looked at exactly the same field of view, with the same amount of cloud element resolution, and made no error in estimating cloud cover. In other words, they are caused by observer dependent difficulties in estimating cloud cover precisely. However, earth-viewing missions are also affected by another aspect of cloud cover which is not treated at all by ground observers - cloud shadow. In conventional observations, cloud shadow is not measured nor is it considered important in most areas of meteorological research.

For satellite studies of terrestrial features, on the other hand, it is very important, for cloud shadows can obscure the surface at visible wavelengths just as effectively as the clouds themselves.

The purpose of this current study was thus twofold. First, the goal was to re-evaluate the relationship between satellite and ground observed cloud cover using photographs from LANDSAT 1. The sensors on-board this satellite have a much higher resolution than cameras used for previous cloud cover correlations (e.g., the NIMBUS 2 AVCS and APT) and thus hopefully show a closer relationship to ground-based measurements. Second, the goal was to determine the effect of cloud shadow on total cloud cover and to evaluate the factors upon which cloud shadow amounts are depenuent.

2.1 The Basic Data Sets

Two data sets were used to perform the above analyses. The first set, used for a comparison of satellite and surface observations, con-sisted of forty-five pairs of LANDSAT photographs, analyzed for 1/4° and 1/2° circles above reporting stations, and concurrent "Service A" and "Service C" observations obtained from the National Weather Service. As is shown in Figure 2-1, these cases are primarily located in the North-east and the Northwest with a number of other stations selected from the South, Midwest and Southwest. They are thus representative of several cloud climatological regions, and, since the months analyzed include January through August, they are also representative of the various cloud conditions associated with different seasons and latitudes.

The second data set, used for an analysis of cloud shadow effects, included the LANDSAT photographs used in the above data set, plus a number of other photographs for which no surface observations were readily available. This data set expansion was of particular importance in analysis of cloud shadow versus sun elevation angle because all LANDSAT-1 observations are made near 1000 LST. Only by the inclusion of a wide variety of latitudes and seasons could the needed variability in sun elevation be provided and the problem of cloud shadow be adequately treated.

Figures 2-2 and 2-3 show LANDSAI photographs typical of the cloud conditions analyzed. The first photograph includes Tucson, Arizona, and

4
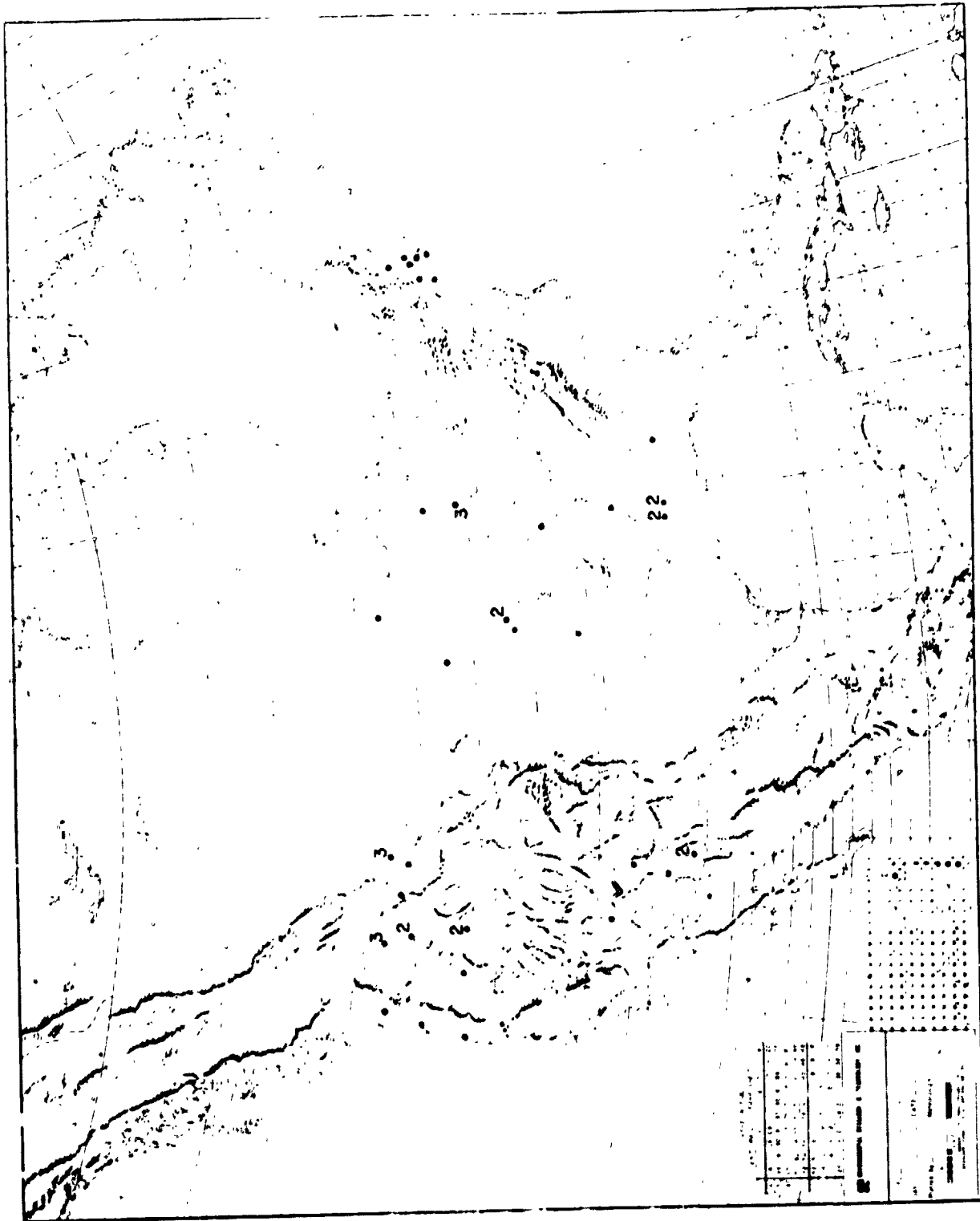
Figure 2-1 Location of Stations Selected for Comparison of Satellite and Surface Cloud Observations

Figure 2-2   LANDSAT-1 Photograph of Arizona, 31 January 1973
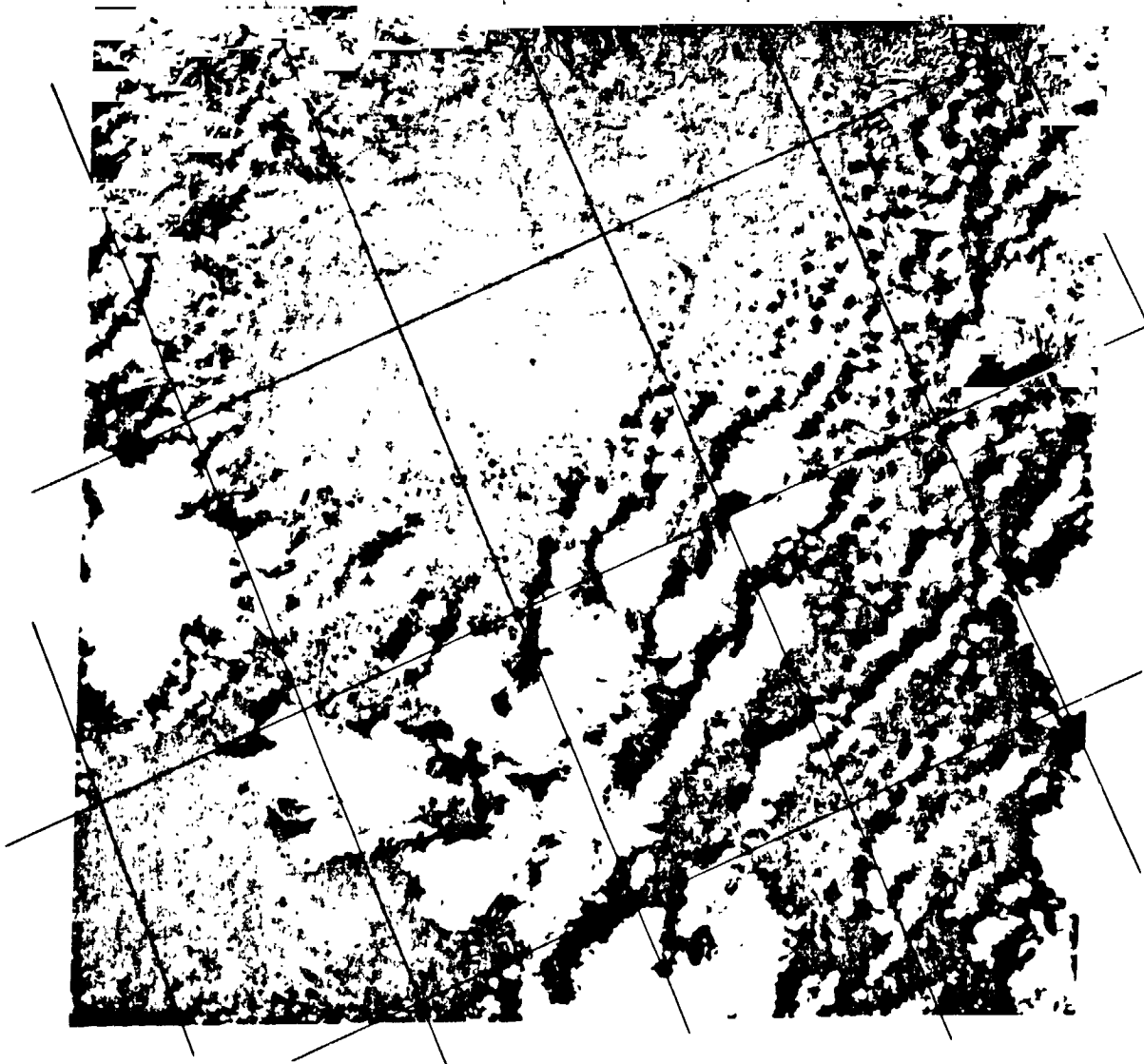
Figure 2-3   LANDSAT-1 Photograph of Northwestern Canada,
            10 January 1973

illustrates clearly several of the difficulties encountered in comparing satellite and stations observations. The clouds are broken and scattered, and changing rapidly with convective growth. Thus, this photograph, taken at 1728Z probably shows conditions not identical to those observed from Tucson at 1700Z or 1800Z, although the measurements of total cloud cover are consistent with time and agree well with the satellite's. Many cases originally selected for analysis had to be discarded because of a lack of stability in cloud conditions (e.g., moving frontal clouds) and a lack of agreement in reporting times, which meant that the surface and satellite observations were not made of the same cloud situations. On the other hand, cases which had differences due to observer dependent problems (e.g., obscuration of upper layers by lower clouds, or coverage by very thin cirrus) were retained to provide a representative sample for comparison.

Figure 2-3 shows a photograph of northwestern Canada (approx. 68°N, 140°W) used only for the cloud shadow analysis. Taken on 10 July 1973 at a sun elevation angle of 43°, this picture shows pronounced cloud shadows from the large cumulonimbus developing in the area. Comparison with Figure 2-2, taken at an elevation angle of 32°, shows some sun angle effects, but it also clearly demonstrates the relationship between cloud height and cloud shadow. In both figures, it is the cirrus or the large cumulonimbi which throw the greatest shadows while the tiny cumulus throw the least shadow. However, as the sky becomes increasingly covered by clouds (e.g., lower right, Figure 2-2), the cloud shadow effect lessens until 100% coverage is reached and no shadow is seen. Measurement of area cloud cover and cloud shadow cover were thus made independently and the ratios of the two percentages were derived for analysis. These measurements were also grouped into categories of low, middle, and high clouds with photographs carefully chosen to minimize the range of heights within cloud height categories.

2.2 A Comparison of Satellite Observed Cloud Cover with Surface
     Observed Cloud Cover

The forty-five pairs of satellite and surface observations discussed above provided measurements of:

- Surface cloud cover percentages

- Satellite observed cloud cover percentages for 1/4° latitude (15 n mi.) circles around the reporting stations

- Satellite observed cloud cover percentages for 1/2° latitude (30 n mi.) circles around the reporting stations

- Satellite observed cloud cover plus cloud shadow percentages for the same 1/4° circles

- Satellite observed cloud cover plus cloud shadow percentages for the same 1/2° circles.

No measurements were made of the cloud cover observed within a 1° circle because of the high resolution and small field of view of the LANDSAT sensor. Most photographs covered an area approximately 1-1/2° latitude by 1-1/2° longitude, and it was rare that a station was so centered that a 1° circle around it was contained in one picture. Previous studies of cloud cover emphasized a comparison of 1/2° and 1° area cloud cover measurements (e.g., Greaves et al, 1971) in order to take the surface cloud cover observations, corresponding generally to a 30 n mi. field of view, and convert them to 60 n mi. corresponding to a satellite field of view. In this study, the goal was more to see how well the 1/2° satellite observations agreed with the surface observations and to see what correlation the surface measurements would show with an even smaller field of view, that of 15 n mi.

The cloud cover percentages for the four sets of satellite analyses were regressed against the surface cloud cover amounts to derive second and third order polynomials expressing the relationship between satellite and surface observations. Figures 2-4 and 2-5 show the resulting curves along with the original data points used. In Figure 2-4, comparing the 1/4° field of view with the surface observations, the cloud cover amounts tend to cluster around certain values. The satellite sees very little (< 5%) cloud cover until surface reports indicate up to 25% coverage, then agrees well with the surface observations up to 75% coverage. For higher cloud cover amounts, the satellite often indicates 5 to 10% greater coverage than is seen from the ground, but in general there seems to be little observer discrepancy under overcast conditions.

Figure 2-4   Comparison of Satellite Observed Cloud Cover for
1/4° Field of View with Surface Observed Cloud
Cover

10
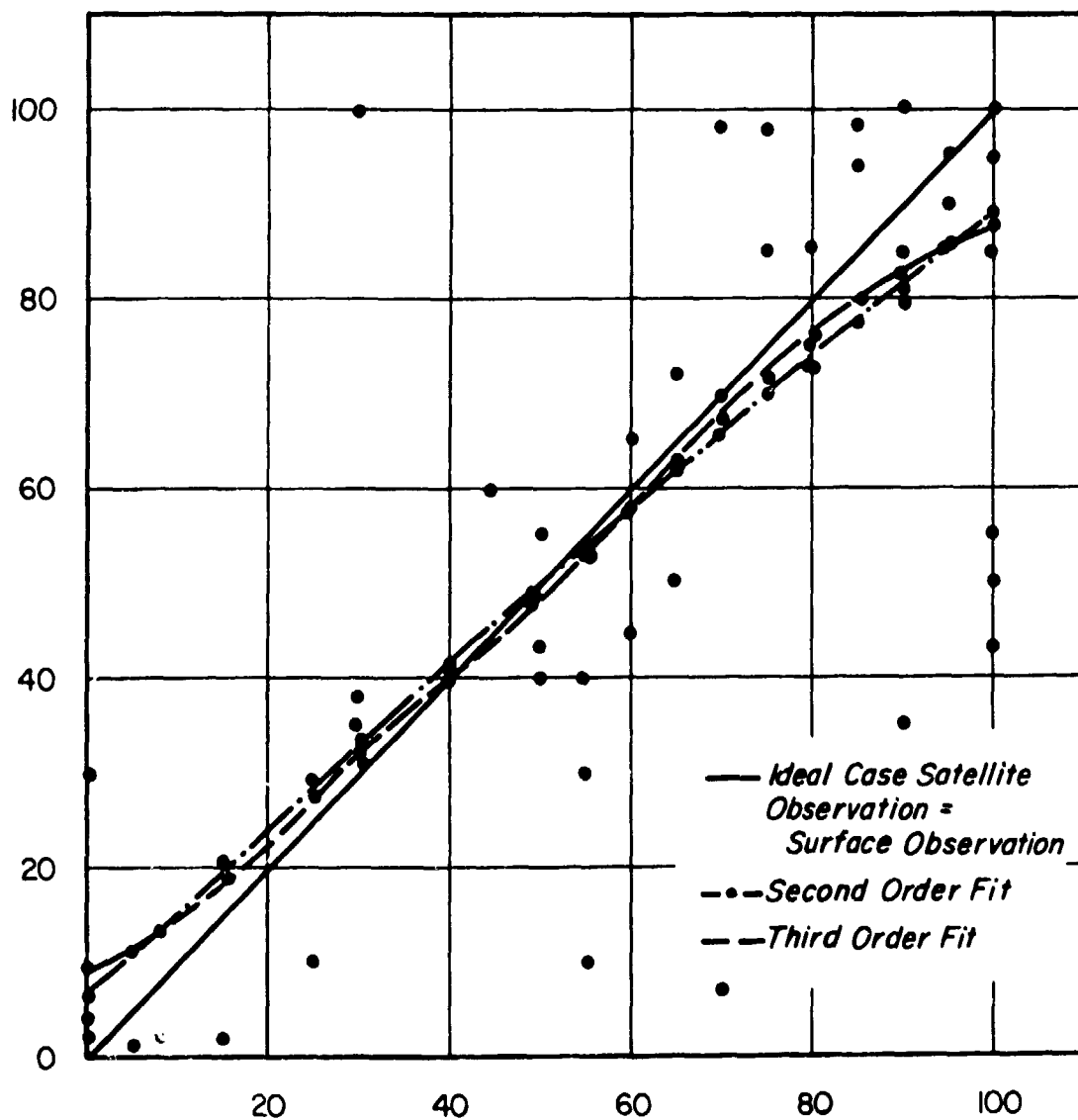
Figure 2-5 Comparison of Satellite Observed Cloud Cover for 1/2° Field of View with Surface Observed Cloud Cover

Scatter in the data points offset some of these trends in the curve fitting, but it was difficult to determine whether these values reflected actual observer differences or pronounced changes in cloud cover between the two observer times. Since the points became more clustered as the data sample increased, it may be that a larger data sample will show these observations to be spurious. (In most cases of pronounced differences in observed cloud cover, e.g., cloud covers 100% satellite versus 30% surface or 50% satellite versus 100% surface, the sky conditions were in a state of rapid change, and it was impossible to determine what occurred ten minutes before or after the photo.) However, Figure 2-4 indicates that the 1/4° satellite field of view shows slightly higher cloud cover than the surface observer sees up to 20% coverages, then 5 to 10% less coverage up to overcast conditions.

Figure 2-5 shows similar information for cloud observations made with a 1/2° satellite field of view. There is slightly less cluster of the data here, though, and the satellite observations show generally good agreement with the surface. The curves generated by the least squares fit reflects the fact that this field of view is the optimum for comparison - less than 5% difference in cloud cover is found for coverages between 20% and 80%. Again the regression analysis indicates that the satellite overestimates coverage for nearly clear skies and underestimates it for overcast conditions. These results are in good agreement with those found by Barnes and Chang (1968) using 1/2° analyses from NIMBUS II APT photographs. The data they regressed also showed that the satellite overestimates for low cloud coverage, underestimates for high coverage and generally matches surface observations for 3 - 7 tenths coverage. However, the current data sample does show slightly better correlations between the two sets of observations; in fact, surface cloud cover amounts appear to simulate well LANDSAT observations for 1/2° areas, and, with a slight reduction in cloud cover percentages, can also be readily applied to 1/4° areas.

The cloud cover amounts analyzed above were measurements of the coverage by clouds only. The same set of satellite photographs were also analyzed to obtain measurements of the coverage provided by clouds plus cloud shadow. Figures 2-6 and 2-7 show these observations and the regression curves derived by the least squares fit, while Figure 2-8
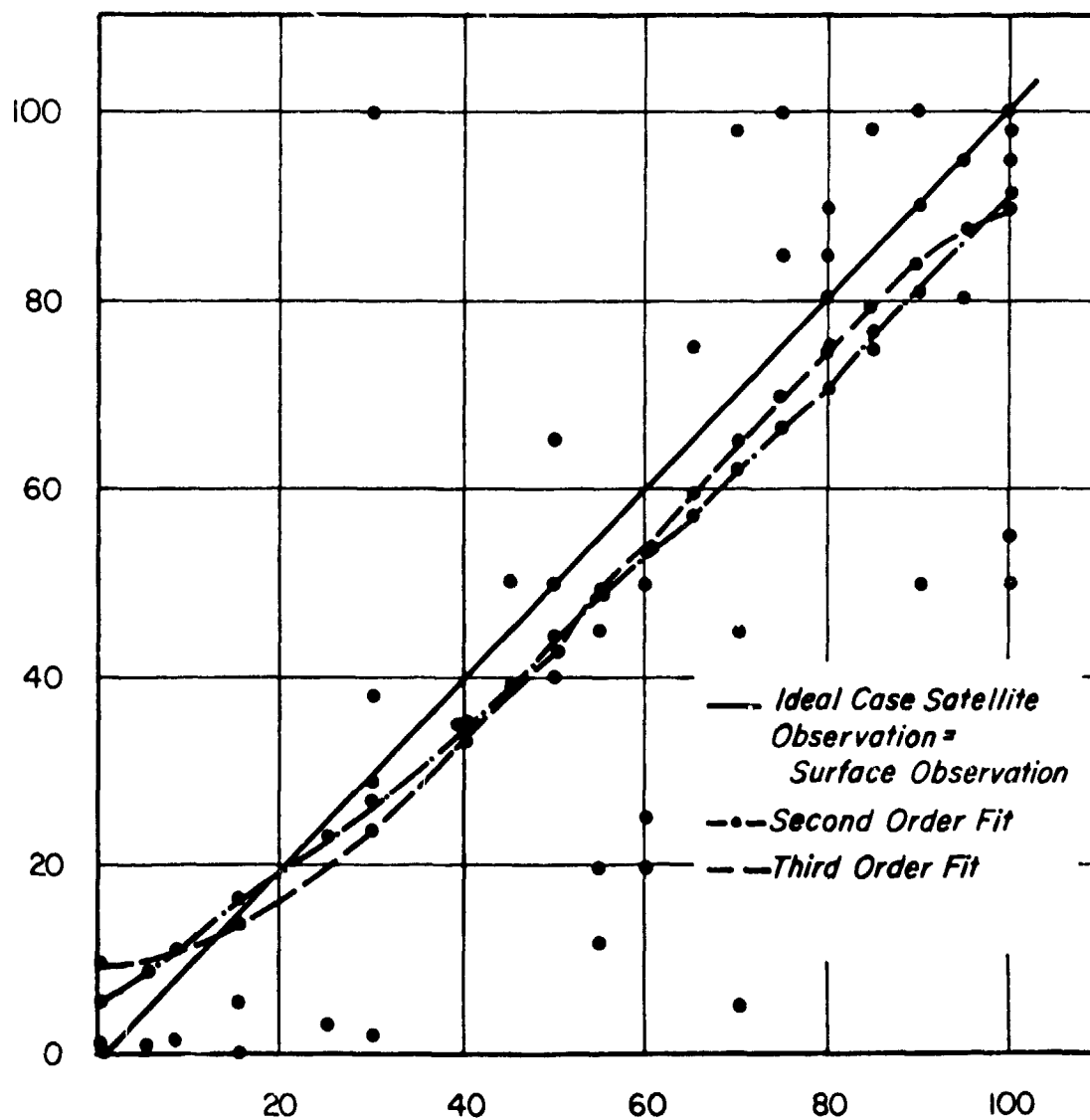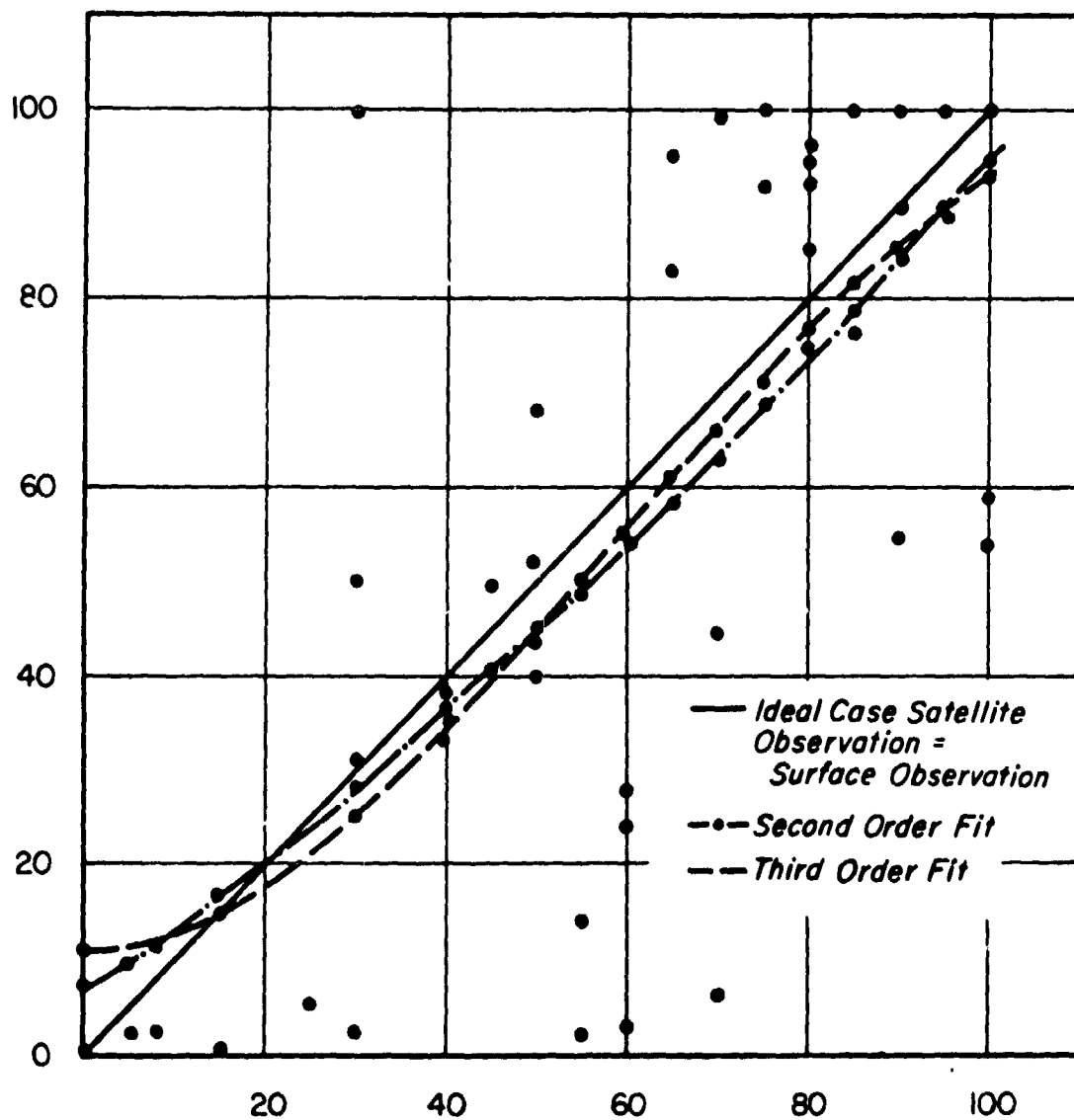
Figure 2-6   Comparison of Satellite Observed Cloud Cover Plus
Cloud Shadow for 1/4° Field of View with Surface
Observed Cloud Cover
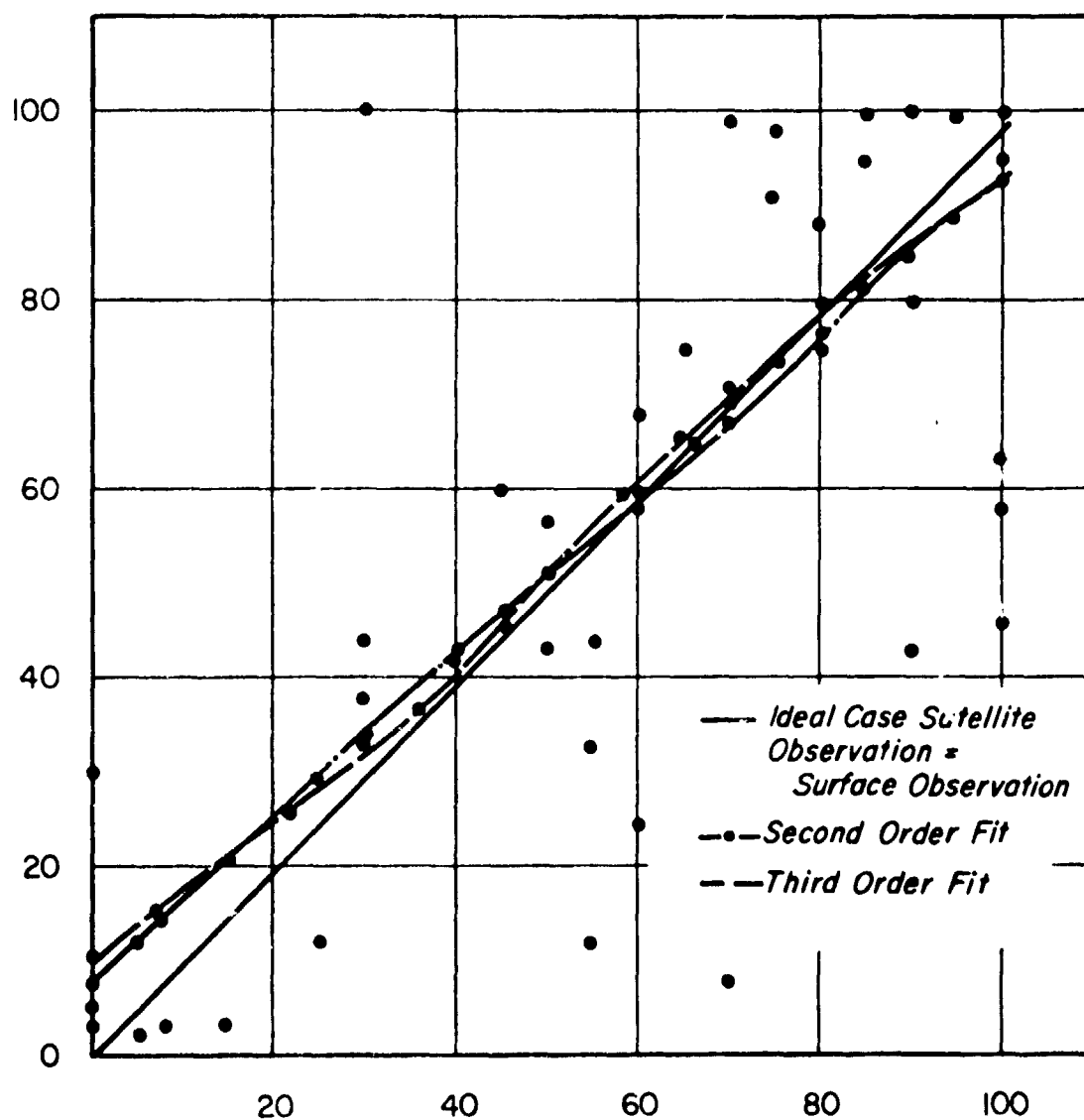
Figure 2-7   Comparison of Satellite Observed Cloud Cover Plus
Cloud Shadow for 1/2° Field of View with Surface
Observed Cloud Cover

14
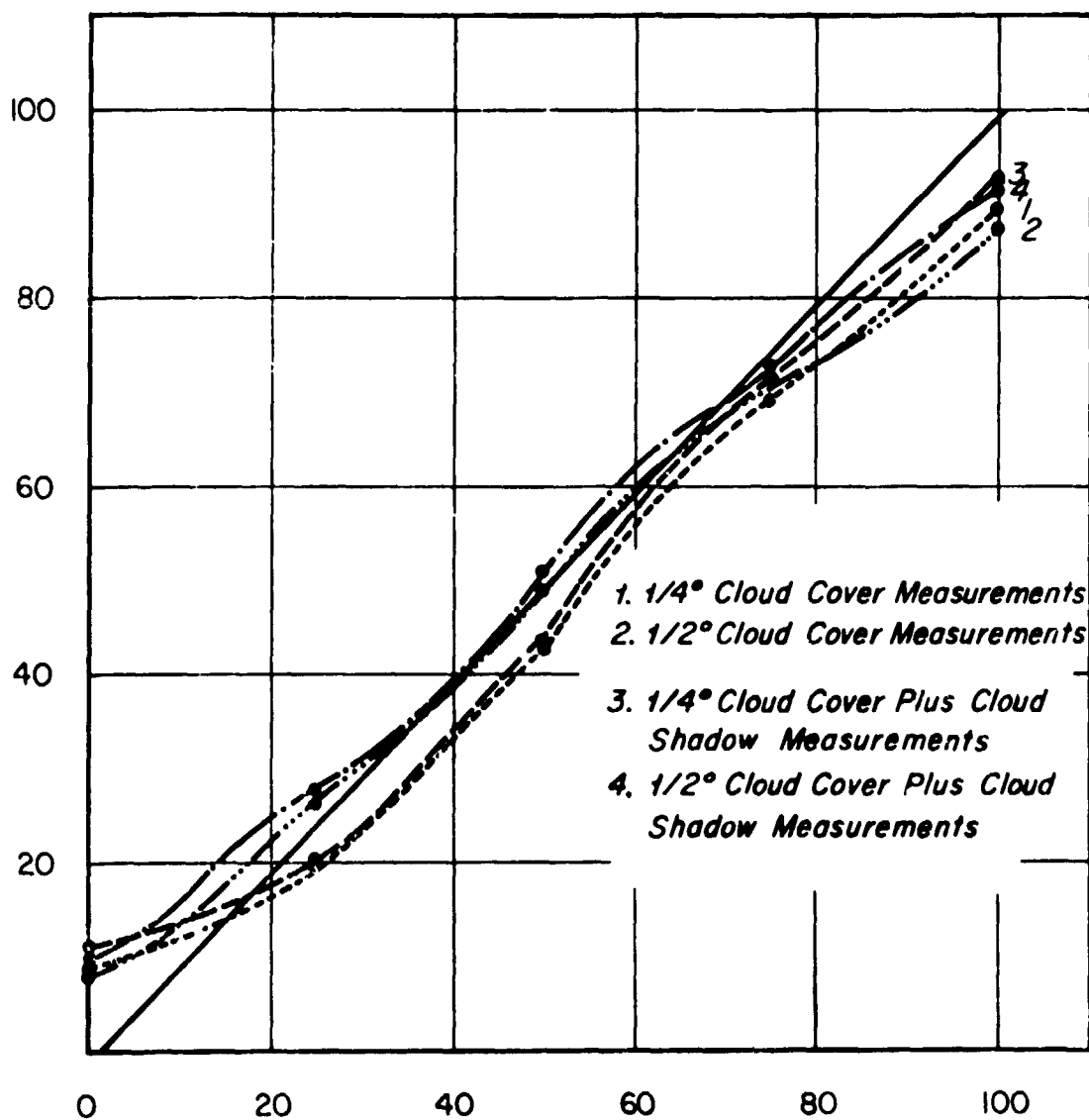
Figure 2-8   Derived Relationships Between Satellite and
Surface Observed Cloud Cover

shows the third order curves generated by the four samples. As would be expected, the overall trend in the relationship between satellite and surface cloud cover observations remains unchanged, but the coverage viewed by the satellite increases. The greatest increase occurs at coverages greater than 75%, and the next greatest changes appear at coverages of less than 20%. This seemed to be the result of the fact that most cloud shadows added less than 5% to the total coverage. Thus, the shadows had the most noticeable effect under nearly clear situations where they could double the coverage viewed and under nearly overcast situations where they could make the coverage go to 100%. For inter-mediate cloud cover amounts, there was enough variability in the initial observations that the regression was rather insensitive to small increases in the observed amounts.

The overall results of the above analysis seems to indicate that simulation of LANDSAT data with surface cloud observations works very well for the 1/2° field of view and is not significantly degraded by cloud shadow effects. It also works quite well for the 1/4° field of view with some adjustment of the predicted cloud cover to allow for the slightly lower cloud amounts seen in this viewing area. However, since cloud shadow effects can be significant in individual cases, if not in statistical simulations, further analyses were performed on the rela-tionship between cloud cover and cloud shadow.

2.3 The Relationship Between Cloud Cover and Cloud Shadow

To derive the relationship between cloud cover and cloud shadow, sixty-two LANDSAT photographs were carefully analyzed to determine the percentage of cloud cover, the percentage of cloud shadow and the ratio of these parameters within selected 1/2° latitude circles. In each case, separate measurements were made of high level clouds, middle level clouds, and low level clouds, and an attempt was made to retain uni-formity of cloud top height for all cases selected in each category. Because of the large temporal and spatial variability of this data set, the sun elevation angle ranged from 17° to 62° and thus provided a good data set for determining the relationship between elevation angle and cloud shadow.

Figures 2-9 through 2-11 show the relationship between the ratio of cloud shadow to cloud cover and the sun elevation angle for low clouds, middle clouds, and high clouds, respectively. For these analyses, the cloud cover amounts used were less than 60%, since the shadow associated with higher cloud coverage is not sensitive to changes in elevation angle. All cloud heights show a very high ratio of cloud shadow to cloud cover for elevation angles less than 22°, a ratio which decreases with increasing angle as one would intuitively expect. However, the relationship between the ratio and sun elevation seems to become more dependent on cloud height with increasing angle, and the elevation angle at which cloud shadows disappear seems to be strongly dependent on cloud height.

The dependence of cloud shadow on elevation angle for cumulus (Figure 2-9) tends to group into three ranges with a ratio of 0.8 to 1 for elevations of less than 22°, ratios of 0.4 to 0.7 for angles between 32° and 44° and 0.05 to 0.15 for angles greater than 46°. The scatter of points for the lower elevation angles indicates a generally inverse relationship of the ratio with the elevation angle and the curve derived from the least squares fit support this trend. However, as the elevation angle exceeds 45°, the data shows little dependence on angles pointing to the equal likelihood of the 0.15 percent cloud shadow for all elevation angles between 45° and 60°. Presumably this ratio would approach zero as the sun approached the zenith, but the transition from constant cloud shadow ratios to no cloud shadow must occur at angles exceeding 62°.

The relationships between percentage of cloud shadow and elevation angle for altocumulus and cirrus show less tendency to cluster within ranges of elevation angle, and in the case of cirrus, an almost linear inverse relationship is found between the two parameters. In both cases, the trend indicates that the cloud shadow will go to zero at lower elevation angles than that indicated by the cumulus data. In fact, the cirrus shadow seems to disappear at the lowest elevation angle, followed by the altocumulus, followed by the cumulus, with this trend supported at angles between 30° and 45° by decreasing percentages of cloud shadow with increasing cloud heights.

17
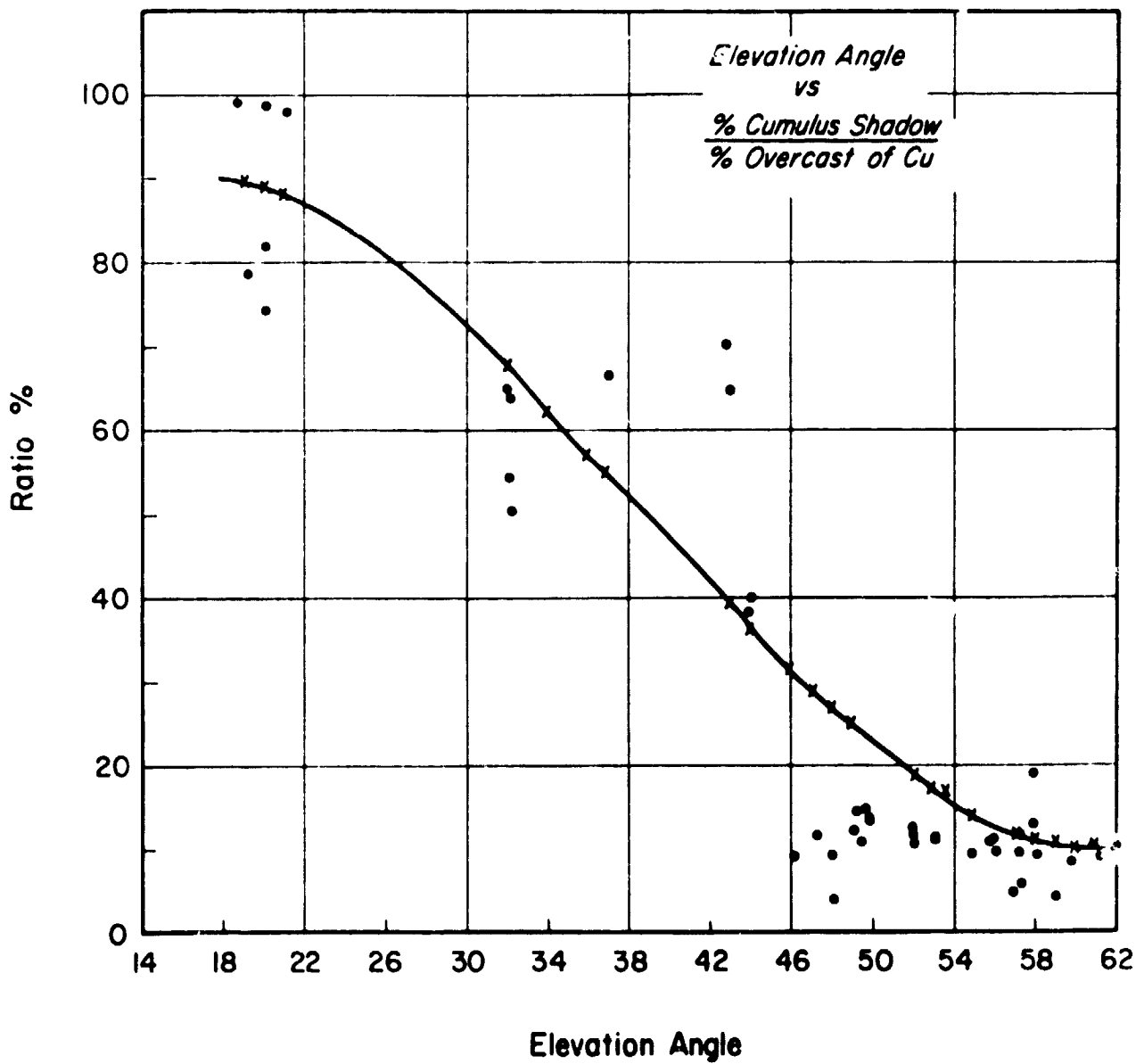
Figure 2-9   The Ratio of Cloud Shadow to Cloud Cover Versus
             Sun Elevation Angle for Cumulus
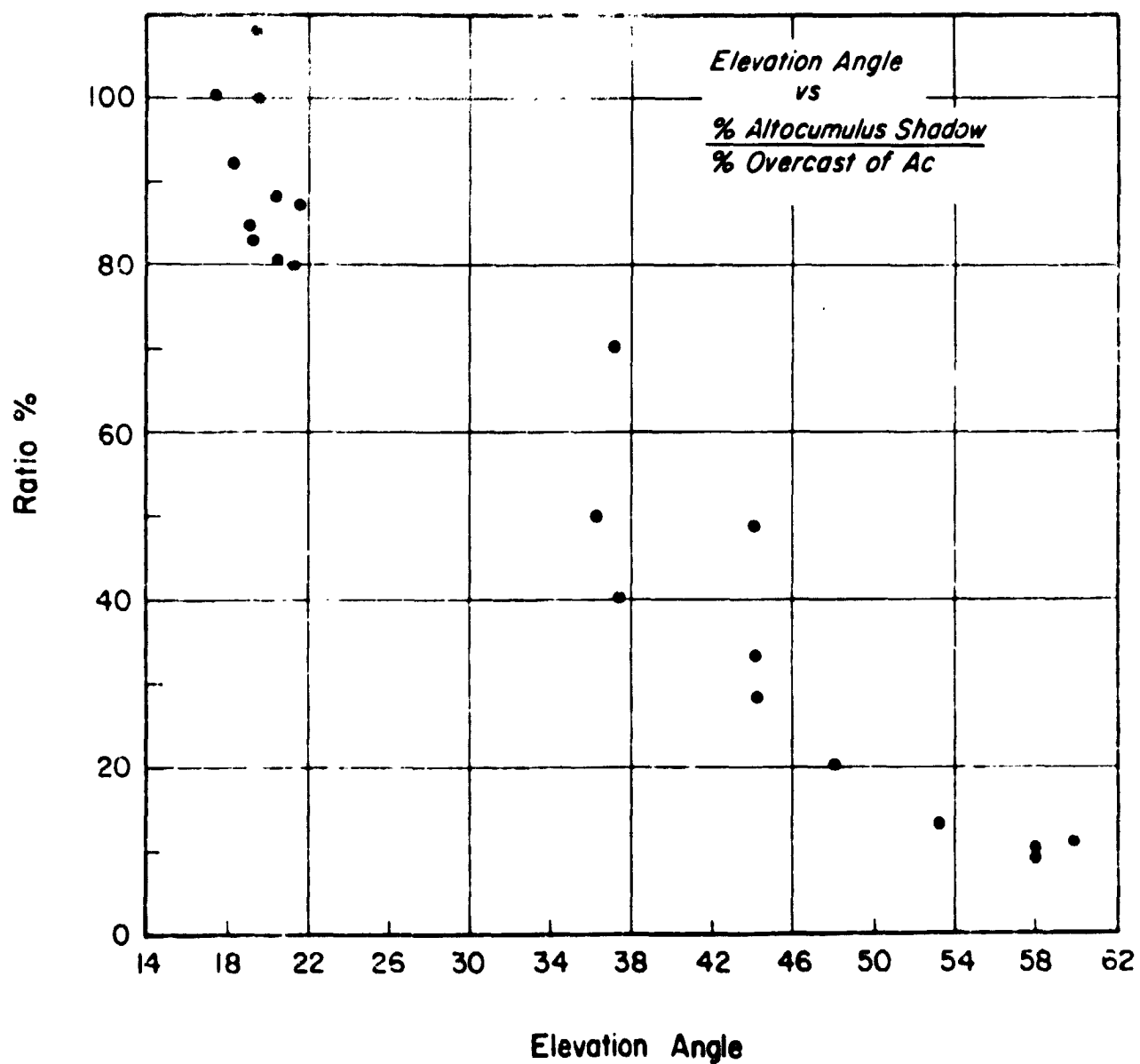
Figure 2-10   The Ratio of Cloud Shadow to Cloud Cover Versus
Sun Elevation Angle for Altocumulus
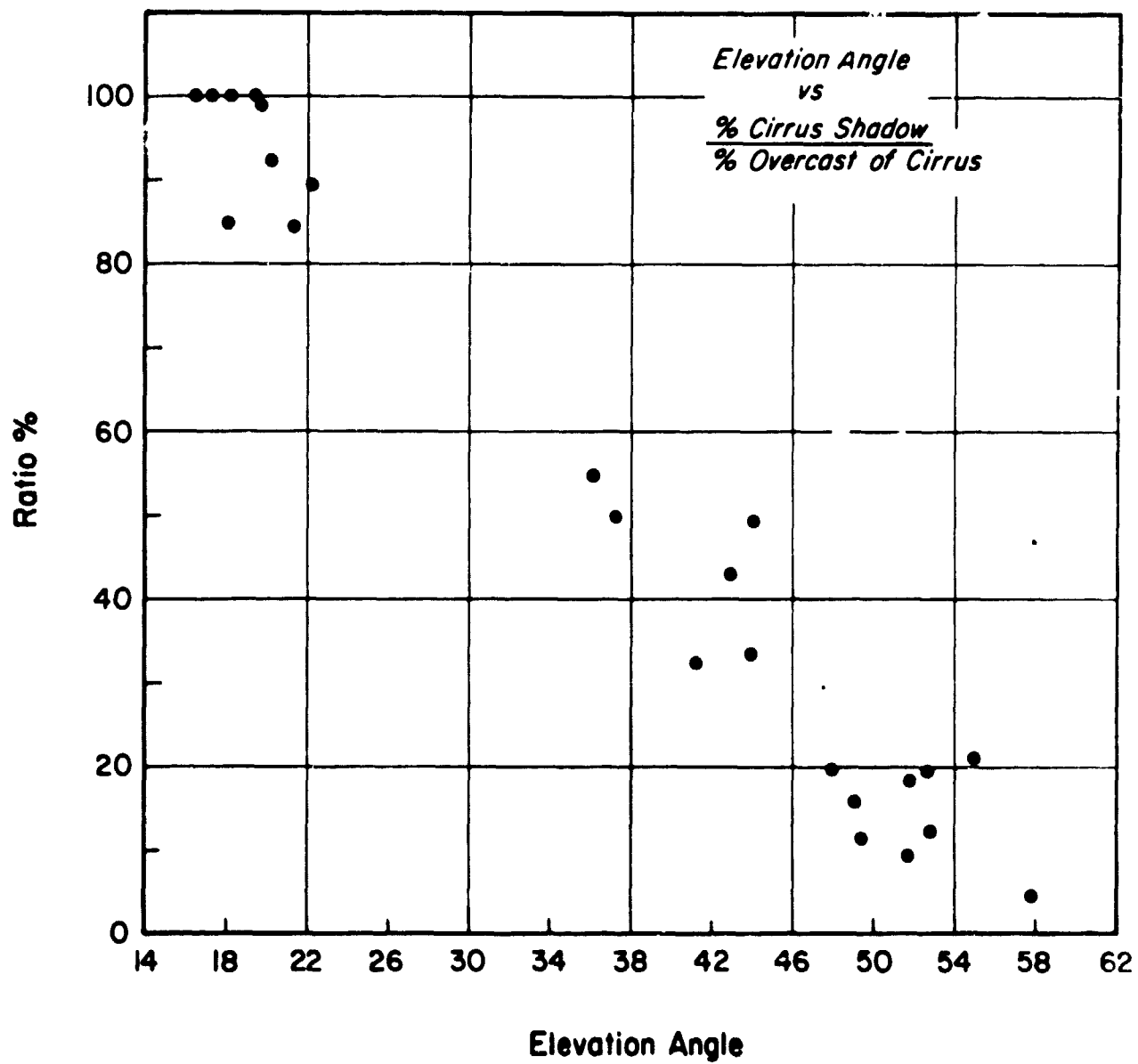
Figure 2-11   The Ratio of Cloud Shadow to Cloud Cover Versus
Sun Elevation Angle for Cirrus

The strong dependence of cloud shadow on elevation angle would seen to contradict the finding in the previous section that the shadow generally adds only about 5% to the total sky coverage. However, there also seems to be a dependence on cloud cover, as illustrated in Figure 2-12 for cumulus. There, most of the cloud coverage is less than 40%, and the highest cloud shadow ratios, corresponding to two elevation angles, seem also correlated with low cloud coverage. The higher amounts of cloud coverage (50%) in general show low cloud ratios - first, because the greater the cloudiness, the less the field of view remaining to show cloud shadows and second, because the higher the cloud coverage, the greater the amount of cloud shadow needed to produce a high shadow to cloud ratio.

In general, then, the highest and lowest amounts of cloud coverage show the smallest increases due to cloud shadow, and the middle range of cloud coverage (20-60%) is the one most likely to have large shadow amounts. In the comparison of satellite viewed coverage with surface viewed coverage, this effect was obscured due to the large scatter in the observers' estimates of cloud coverage and to the combination of data from all elevation angles. Thus, if one wishes to simulate general viewing conditions, the additional 5% increase in coverage due to cloud shadow found in the previous section is quite adequate, but if one wishes to simulate specific sun elevation angles for cloud coverage between 20 and 60%, the dependence of shadow on elevation angle should be evaluated.
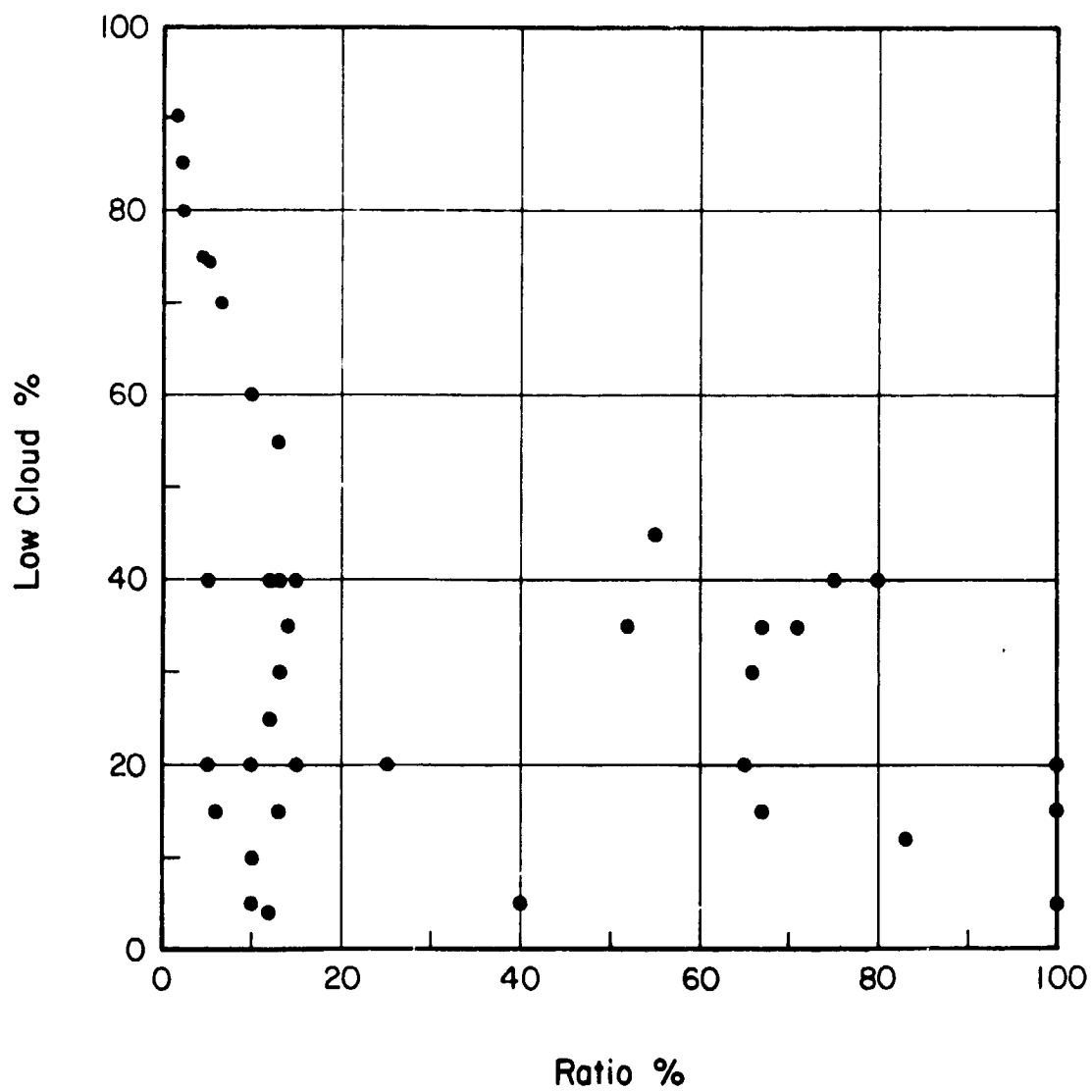
Figure 2-12   The Ratio of Cloud Shadow to Cloud Cover Versus
               Cloud Cover for Cumulus

3. THE STRATOSPHERIC MODEL

To supplement the global cloud model in meeting the requirements for remote sensing studies of the earth's surface, a global atmospheric model was developed by Spiegler and Greaves (1971) and Spiegler and Fowler (1972). This model, known as the 4-D model, provides monthly means and variances of pressure, temperature, water vapor and density at 1 km levels from the surface to 25 km for any location on the globe. These values have proved useful in defining expected atmospheric conditions along suborbital tracks, and have been applied to the study of water vapor attenuation at infrared wavelengths (Chang and Fowler, 1973).

Since the development of this model, however, the emphasis in planning space missions has shifted from determining the attenuation of radiometric sensors by the lower atmosphere to defining the effects of of the stratosphere and upper atmosphere on space vehicles. This is of particular importance in the design and development of the space shuttle program, for a thorough knowledge of the upper atmosphere is needed in anticipating density perturbations and in computing trajectories and aerodynamic heating. Thus a comprehensive statistical representation of atmospheric conditions from the surface to 185 km was developed by Justus, Roper and Woodrum (1974), combining empirical models such as the 4-D model and Groves (1971) model.

The Groves model consists of monthly values of atmospheric parameters at 5 km levels from 25 to 110 km for 10° latitudinal bands across the globe. However, because of the limited data set available for analysis, the model did not attempt to include either daily or longitudinal deviations from the monthly values. Thus, though it gives an excellent representation of the stratosphere and mesophere, it is limited in the amount of information it provides for evaluating expected changes in atmospheric parameters along a reentry path.

The purpose of this phase of the study was the extension of the 4-D model through the stratosphere to provide atmospheric statistics similar to those generated for the troposphere and lower stratosphere. In particular the goal was to derive empirically monthly means and daily variances of pressure, temperature, density and winds at 2 km levels

23

from 26 km to 52 km. These values would be given at grid points across the globe to permit an evaluation of the spatial as well as temporal changes in the stratosphere.

Examination of the rocketsonde data available for analysis soon led to the realization that the derivation of grid values across the entire globe is not yet possible. Very few rocketsonde stations are located in the eastern half of the Northern Hemisphere and there are even fewer stations in the Southern Hemisphere. Hence it was decided to concentrate on the area in the western northern hemisphere from 0° longitude to 160° east longitude. This zone includes most of the Meteorological Rocket Network and thus has the largest collection of stratospheric measurements. Further data collection is still needed to provide a satisfactory base for grid statistics; however, the available soundings did allow generation of monthly statistics of the important atmospheric parameters at a large number of stations. These statistics were then analyzed spatially to produce constant level maps from which values were read at 5° latitude - longitude inte sections, and interpolated vertically to provide stratospheric profiles. The following section will discuss in more detail the data processing and analysis.

3.1 Rocketsonde Data Processing and Analysis

The stratospheric data set consisted of rocketsonde measurements made by stations in the Meteorological Rocket Network (MRN). These values were obtained from the World Weather Center A at Asheville, North Carolina and were formatted as follows:

- Summed meteorological parameters (sums, sums of squares and counts of pressure, temperature, density, and u and v wind components) at 1 km levels for 18 stations in the MRN network for the period 1969 - 1972.

- Summed meteorological parameters at 1 km levels for 6 stations covering the period 1961 - 1968.

- Daily rocketsonde values for Russian, Asian, and European stations covering the period from 1969 - 1972.

TABLE 3-1

ROCKETSONDE STATIONS USED IN STRATOSPHERIC ANALYSES

Station Number	Name	Latitude Longitude	Period of Record	Number of Observations
0-10°N				
78783	Fort Sherman	09.3 N 080.0 W	69-72	374
43373	Thumba	08.5 N 076.64 E	70	19
10-20°N				
78861	Antigua	17.2 N 061.8 W	69-72	287
91250	Eniwetok	11.4 N 162.4 E	66-67	20
20-30°N				
74794	Cape Kennedy	28.5 N 080.5 W	69-72	717
			64-68	1.110
91162	Barking Sands	22.0 N 159.8 W	69072	683
30-40°N				
08384	Arenosillo	37.1 N 006.7 W	69-72	84
72269	White Sands	32.4 N 106.5 W	69-72	913
			61-68	1,889
72391	Point Mugu	34.1 N 119.1 W	69-72	772
			61-68	1,285
72402	Wallops Island	37.8 N 075.5 W	69-72	672
			61-68	844
72477	Green River	38.9 N 110.1 W	69-72	32
47517	Akita	39.33 N 14.0.2 E	70-72	74
40-50°N				
34560	Volgograd	48.68 N 44.35 E	65-70	140
50-60°N				
72913	Fort Churchill	58.7 N 093.8 W	69-72	536
74124	Primrose Lake	54.8 N 110.1 W	69-72	298
03023	West Geirinish	57.35 N 007.36 W	69-71	117
03502	Aberporth	52.13 N 004.57 W	71	19
60-70°N				
70192		65.1 N 147.5 W	69-72	433
70266	Fort Greely	64.0 N 145.7 W	69-72	380
			61-68	904
70-90°N				
04202	Thule, Greenland	76.6 N 068.8 W	69-72	203
20046	Heiss Island	80.62 N 58.50 E	57-70	218
Southern Hemisphere				
61902	Ascension Island	08.0 S 014.4 W	69-72	543
			64-68	780
82599	Natal	05.9 S 035.2 W	69-72	36
87689	Mar Chiquita	37.8 S 057.4 W	69-72	40
41350	Gan	00.68 S 073.15 E	69-70	64
Mobile Russian Ship Sta.				
M9009-M9209			67-70	319

The actual stations included in this data set, the number of observations available for each station, are listed in Table 3-1. This table clearly shows the two main difficulties in deriving global stratospheric statistics. One is the lack of continuous spatial coverage, e.g. no stations between 40 and 50°N in the western hemisphere, and the other is the lack of a consistent period of record for the reporting stations which can lead to apparent spatial differences in meteorological values caused only by differences in the number of observations or in the months sampled. Throughout this study a major effort was made to minimize the effects of these problems and thus to generate a relatively consistent and reliable data set; however, the problems can not be completely resolved without more extensive observations.

The initial processing took the available data and generated means and variances at 2 km levels for each station from 24 km to 52 km, combining the 1961-68 data sets with those for 1969-72 for appropriate stations. The level below 25 km was chosen to permit comparison of the statistics resulting from the rocketsonde measurements with those in the existing 4-D model while 52 km was selected to provide data for the upward extrapolation of longitudinal variabilities (Justus et al, 1974). The resulting data set also permitted comparison with Groves values at 30, 40 and 50 km although a time shift was necessary as his values were centered on the first day of the month and these were derived for the fifteenth.

Figures 3-1 and 3-2 show the mean temperatures computed from the 1969-1972 rocketsonde data for stations near 30°N for January and July. With these profiles are plotted the Groves temperatures for 30°N. There is very good agreement up to 45 km reflecting the fact that Groves used the same data set, but the values above 45 km seem to diverge for the January data. This appears to be partially caused by the location of the maximum temperature at an altitude between 45 and 50 km and thus between the values given by Groves model, but not between those given at 2 km levels.

These differences also, in some cases, appear to reflect the lack of a data set large enough to be statistically valid. Although the number of soundings listed in Table 3-1 indicates the total number of soundings available for analysis, few of these stations had this number
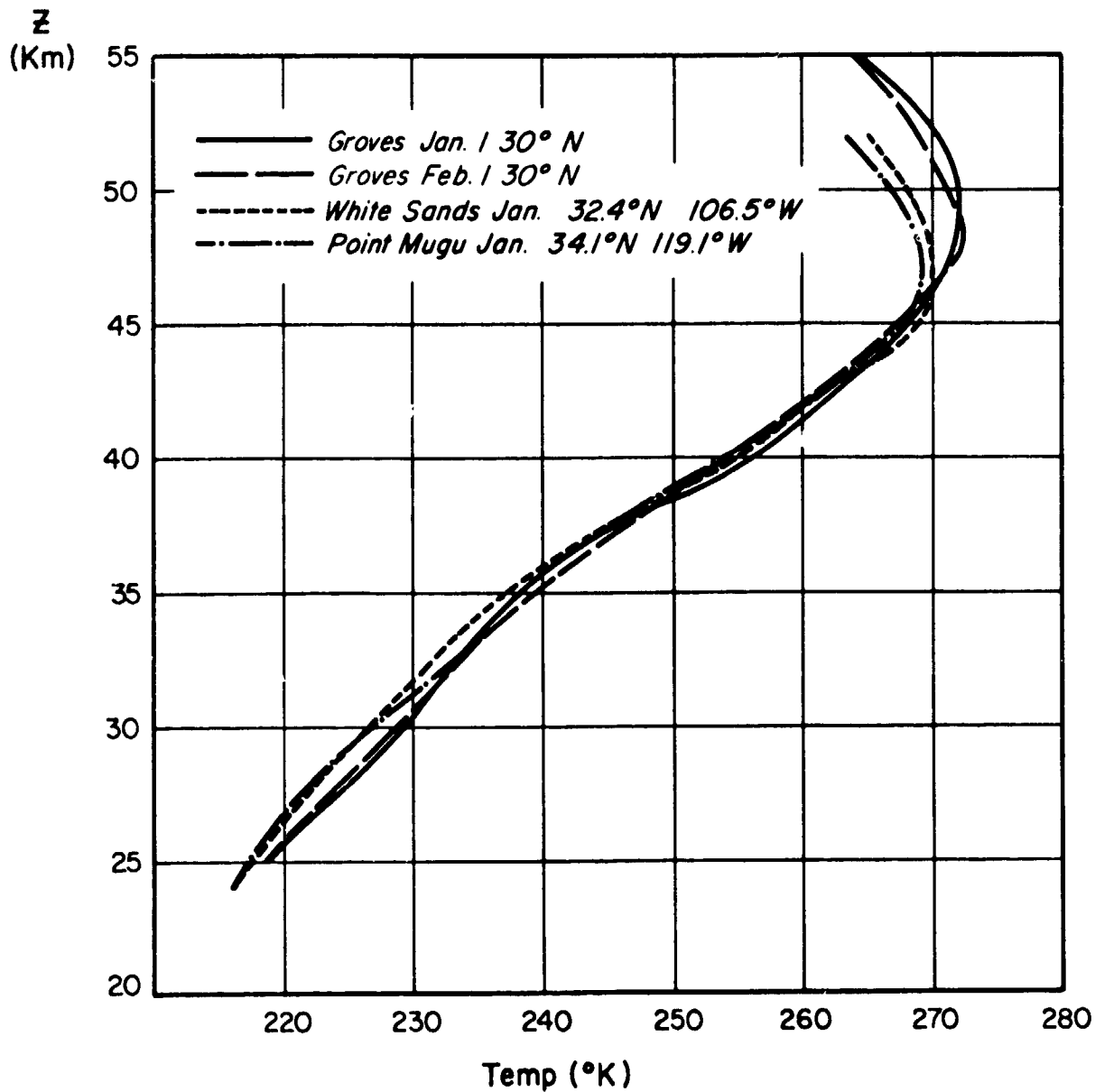
Figure 3-1   Mean Stratospheric Temperature Profiles for
January near 30° N
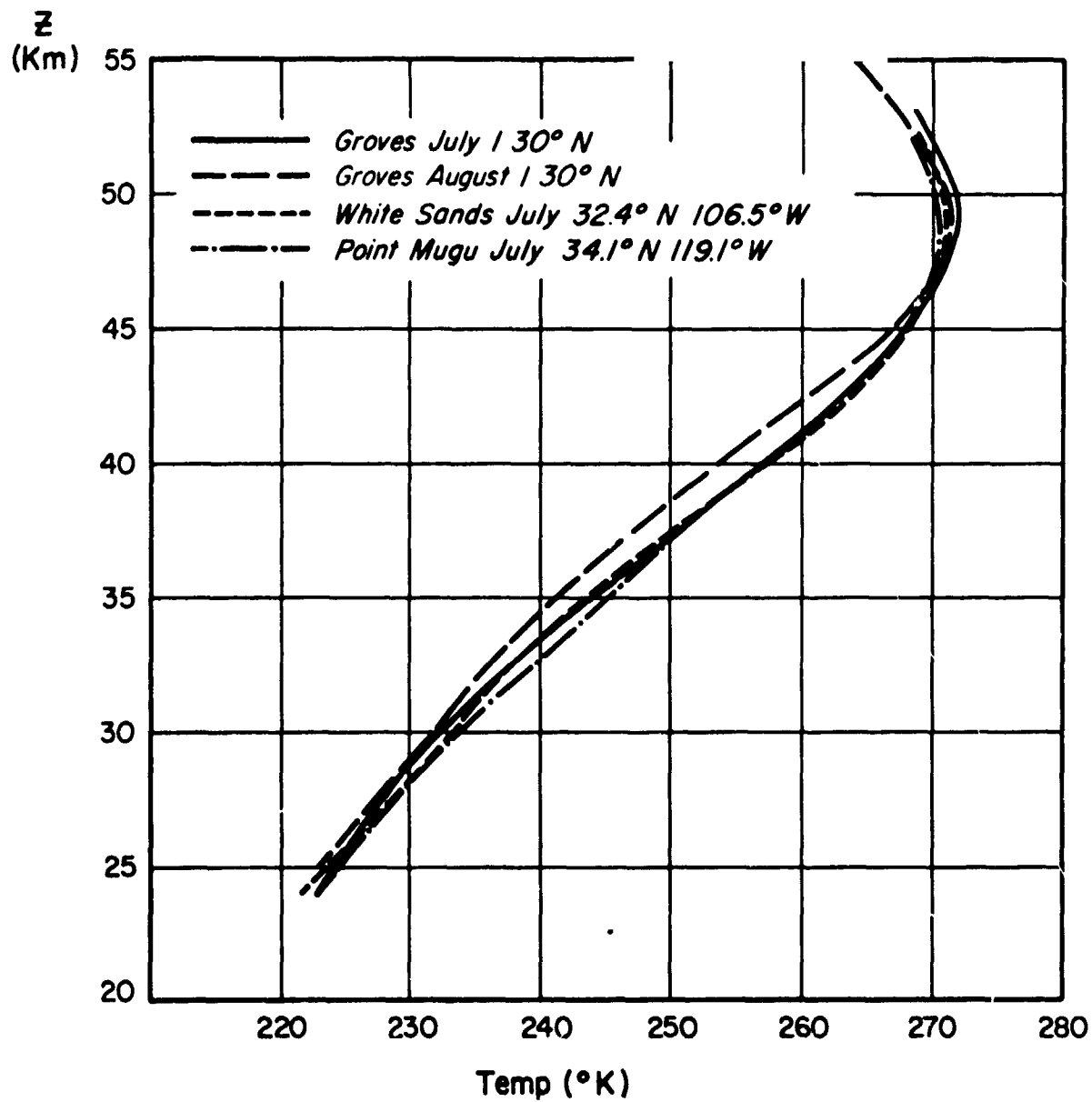
Figure 3-2   Mean Stratospheric Temperature Profiles for
July near 30° N

of soundings for all parameters. In general, the winds had the largest
set of observations with temperature reported significantly less often.
Since temperature can be highly variable and the inclusion of a few
stratospheric warmings can bias the statistics, it is difficult to
derive valid temperature means from the soundings available, especially
for the winter months. The variances in this model are thus of impor-
tance in evaluating expected meteorological values and their variabilities.

Despite these basic difficulties, it is felt that most of the
statistics derived from these soundings are reliable and in concurrence
with analyses made by other investigators. The statistics are the same
as those published by the World Data Center A in the High Altitude Mete-
orological Data reports because they are derived from exactly the same
soundings. Figures 3-3 and 3-4 show comparisons between the monthly
means derived from midlatitude stations and the monthly values given for
those latitudes by Groves. (Throughout this study, positive winds are
from the west or south, and negative from the east or north.) The
largest differences occur during the winter months (November - February)
and reflect the high natural variability in the stratosphere during this
season. However since these analyses and comparisons with other studies
(e.g. Webb, 1969) showed good agreement between our data and previous
findings, it was decided to analyze these statistics to form global
models.

3.2 The Stratospheric Analysis

The derivation of global grid values involved the plotting and
analysis of all the statistics derived for the stations listed in Table 3-1
(with the exception of stations located below 10°S). This created ten
maps per stratospheric level: five for the means of pressure, tem-
perature, density, west-east wind component (u) and south-north wind
component (v); and five for the standard deviations of the same para-
meters. Time and financial constraints did not permit the plotting and
analysis of this number of maps for all of the 2 km levels for which the
rocketsonde statistics were computed. Thus four levels were selected
for initial analysis: 26 km, 36 km, 42 km and 52 km. These levels were
chosen to provide the values at the base and top of the 4-D model
extension and to provide comparison with previous analyses made at

29
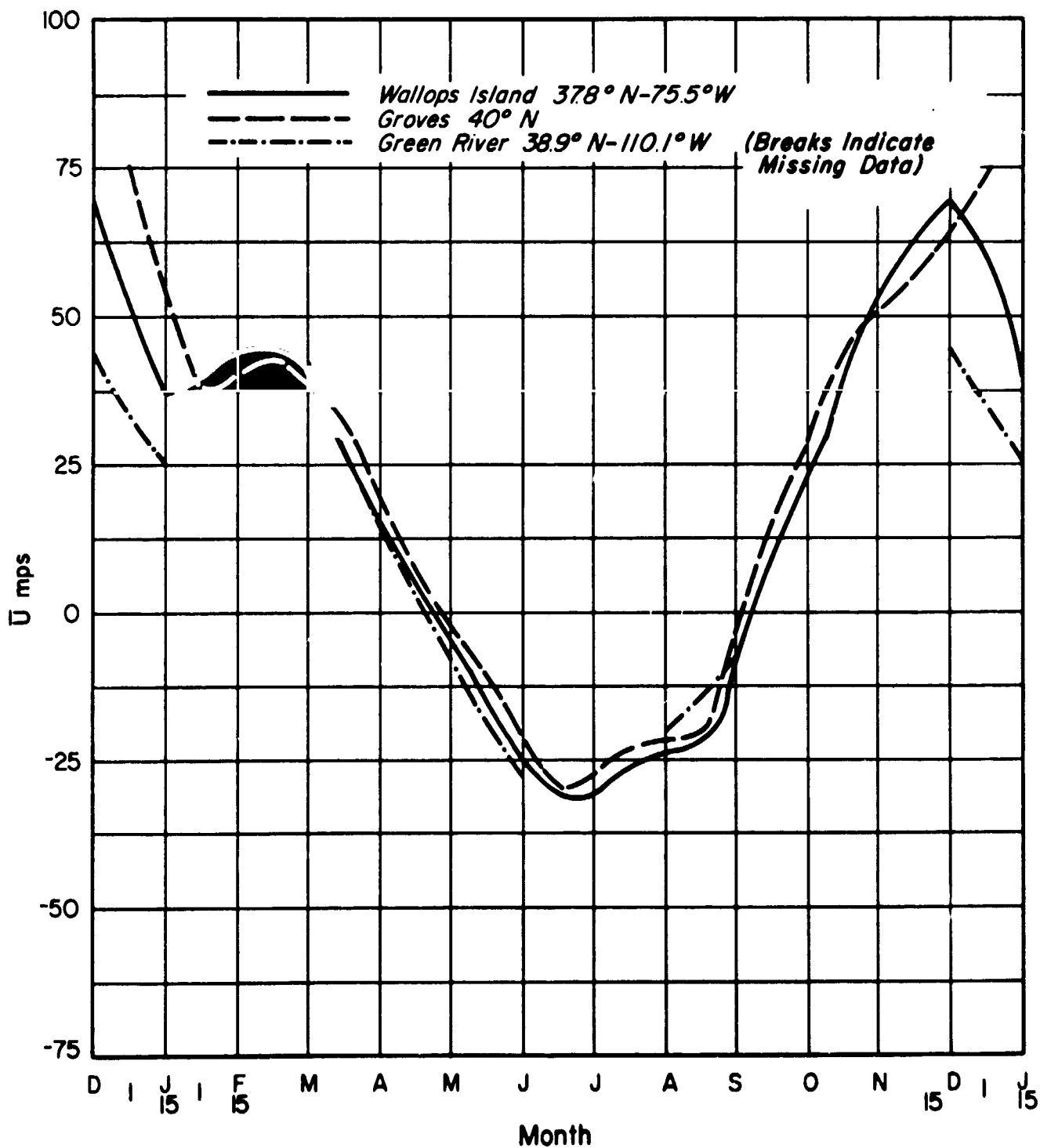
Figure 3-3 Monthly Mean Values of the West-East Wind
Component at 40 km near 40° N
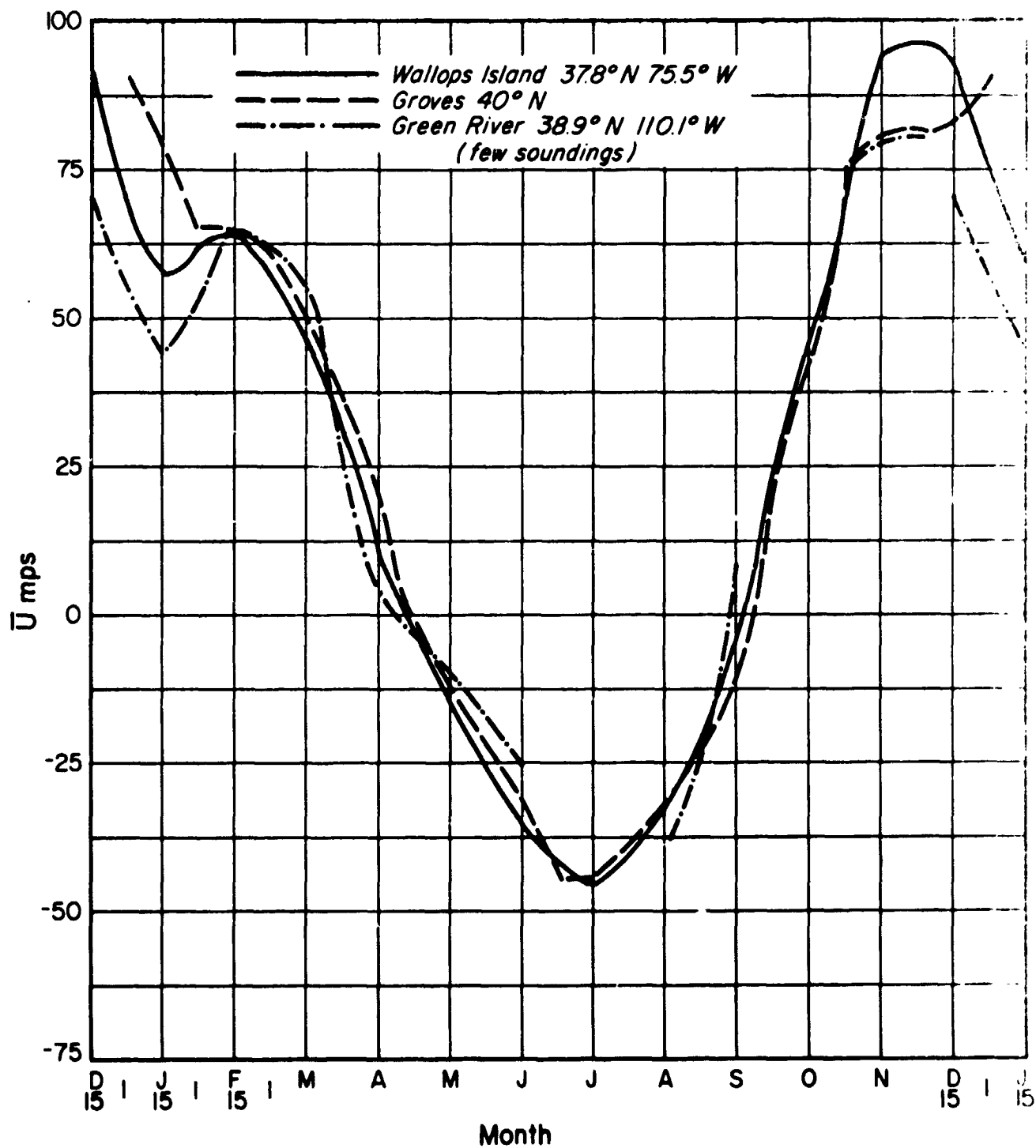
Figure 3-4   Monthly Mean Values of the West-East Wind
Component at 50 km near 40° N

10 mb, 5 mb, 2 mb and .4 mb. Subsequently the level of 48 km was also chosen for analysis to add needed information on the stratopause. Study of the station profiles showed that these five levels should provide good representations of vertical structure of the stratosphere since changes in the statistics between these levels are relatively linear.

Figures 3-5 through 3-8 show the 42 km analyses of temperature and the west-east wind component for January and July. The scarcity of reporting stations necessitated careful subjective analyses over many areas such as the tropical regions, but the seasonal trends and stratospheric patterns are clearly evident. January is characterized by very high variability in both time and space. The most pronounced variability is seen in the January flow patterns (Figure 3-5) for the area between 30°N and 50°N where sudden outbreaks of arctic air and pronounced stratospheric warmings cause very large shifts in the winds in a period of a few hours. On a long-term basis the mean mid-latitude winds show a strong westerly flow pattern, but the standard deviation of this mean clearly demonstrates that the daily winds may show little similarity to the mean. In fact it has been suggested (Belmont et al, 1975) that the mean wind value could be misleading because the actual wind values might not even show a Gaussian distribution.

Other latitudes in January show an easterly flow pattern especially in the eastern polar region and in the tropics and subtropics. The data from the tropical region indicates a relatively stable flow with limited changes in time or in longitude. On the other hand the Arctic region is highly variable and the easterly flow for longitudes near the Greenwich meridian contrasts sharply with the strong westerly flow found over Siberia. Standard deviations on the order of 25 m sec^{-1} are associated with these winds and reflect the frequent changes of the location of the Aleutian high. The south-north wind components analyzed for this level support these analyses of the west-east wind components with a strong mean southward flow for latitudes north of 50°N and a standard deviation of the flow which exceeds the mean (e.g., Fort Greely, mean v = -23.4 m sec^{-1}, standard deviation = 35.56 m sec^{-1}).

The July winds contrast sharply with the January winds in that all of the flow is easterly and there is very little variation either with
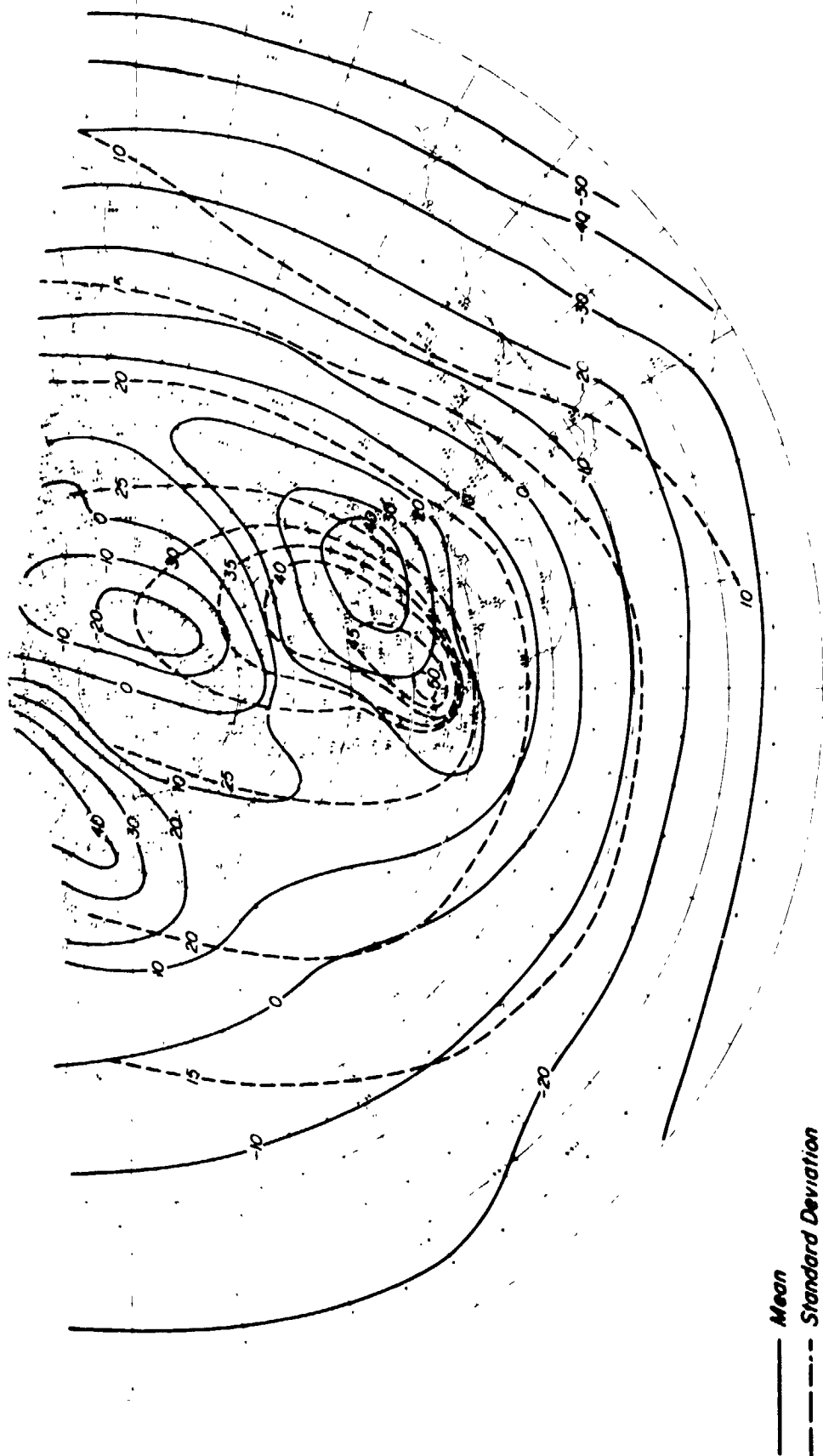
Figure 3-5 Analysis of the West-East Wind Statistics for
January at 42 km

——— Mean
––– Standard Deviation
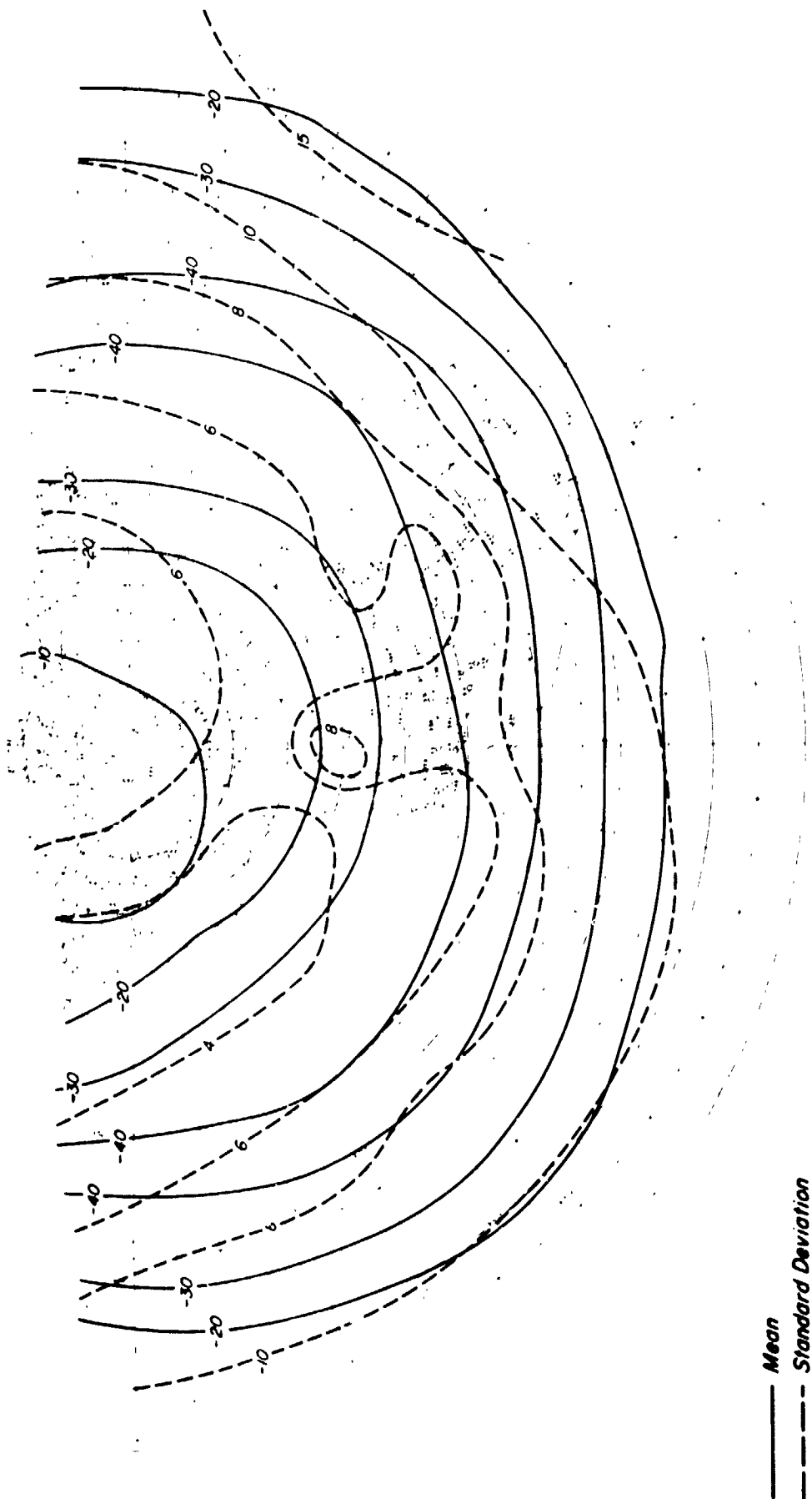
Figure 3-6   Analysis of the West-East Wind Statistics for July at 42 km

——— Mean
——— Standard Deviation
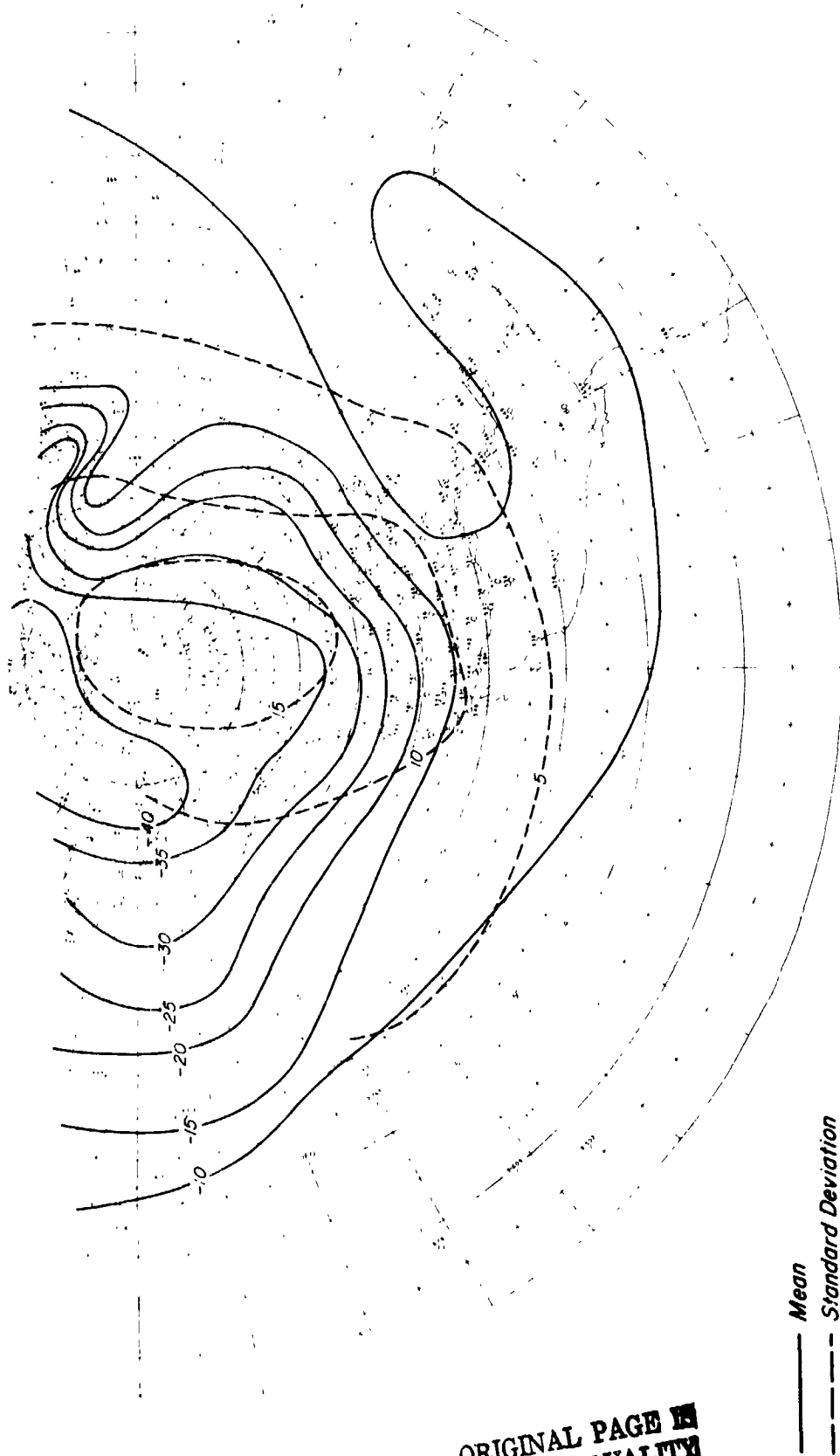
Figure 3-7   Analysis of the Temperature Statistics for
            January at 42 km

——— Mean
- - - Standard Deviation
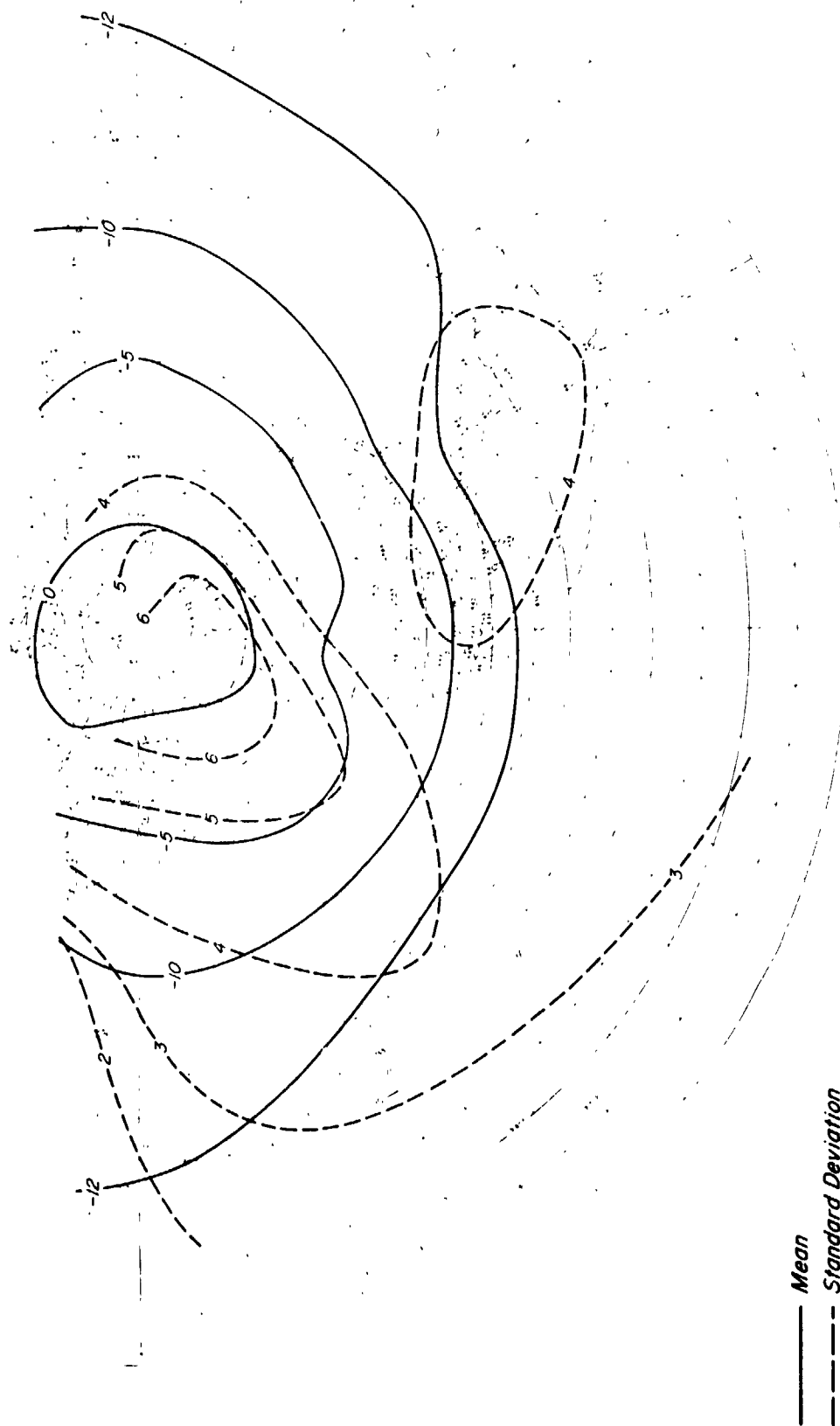
Figure 3-8   Analysis of the Temperature Statistics of July
at 42 km

——— Mean
- - - Standard Deviation

longitude or with time. The maximum winds are found in the zone between 15° and 30°N and the minimum winds are located in the polar region with very weak south-north wind components to interrupt the general flow pattern. For this season the mean winds seem well representative of the daily values making these statistics readily applicable to the modeling of expected stratospheric conditions.

Temperatures shown in Figures 3-7 and 3-8 reflect these sharp seasonal changes with January characterized by sharply decreasing temperatures with increasing latitude, and July by increasing temperatures with increasing latitude. A stronger latitudinal dependence is found for the January temperatures than was displayed by the January winds although the July temperature data appears to have slightly greater longitudinal dependence than the winds showed. An interesting feature of both maps is the correlation of the standard deviation analysis with the north-south flow analyses (not shown). In both seasons the highest variation in temperature occurs in the regions of the strongest southward flow from the arctic region.

Comparison of these analyses with the weekly synoptic analysis charts and the statistics given by Groves (1971), Belmont et al (1975) and other authors shows good general agreement in the basic meteorological conditions characterizing the stratosphere. Specific values for specific latitudes do occasionally disagree, however, due to different time periods used for averaging, the variability found with longitude, varying definitions of representative statistics, and interpretations of the station data. For example, the maximum winds found in the January analysis are less than those given by Groves (1973) but part of the difference can probably be attributed to our definition of the January mean as including all days from January 1-31 whereas his includes days from December 16 to January 15. Much more data is needed to define stratospheric conditions with high precision. Also needed is a standardization of approaches in the empirical modeling of these altitudes. Within these limitations, it is felt that the statistics derived from these analyses provide a good representation of the characteristics and trends of stratospheric circulation.

3.3 Stratospheric Profiles

Since the final goal of this analysis of the stratosphere was the generation of profiles of atmospheric parameters at grid point locations, the analyzed maps underwent further treatment. In this phase, values were read from each map at 10° longitude and latitude intersections from the Greenwich meridian west to 160°E, with the exception of the zone from 65°W to 155°W where values were read at 5° intersections. The data available in this latter region was the densest and it seemed appropriate to obtain the maximum resolution possible. All of the grid point parameters were then keypunched and the 10° grid values were computer interpolated to 5° grid values.

Figures 3-9 through 3-14 show profiles derived from the grid point values at 40°N, 75°W and 20°N, 70°W for January and July. Three parameters are shown, the temperature, u-wind component and v-wind component, plotted against height from 26 km to 52 km. In each figure, the center profile shows the mean value with the other profiles representing values of the mean minus one standard deviation, and the mean plus one standard deviation.

Both seasonal and latitudinal differences are evident in these figures. Not only are the stratospheric characteristics discussed above for 42 km evident (e.g. change in temperature with latitude) but other features are also apparent. The most pronounced difference in the profile is the significantly sharper temperature maximum found at the midlatitude stratopause. In the summer this stratopause also appears lower than it does in the tropics. The greater varibility in the winter temperatures at 40°N is clear, as is the almost uniform variability found over this region in the summer.

The profiles of the west-east wind components reveal a reverse pattern with a sharp maximum wind characterizing the tropical winter profiles and not visible in midlatitude data. Both latitudes show a comparable increase in wind speed with height during the summer but the tropical wind speed, with the exception of the 48 km peak, is almost constant with height in winter while the midlatitude winds increase from 10 to 60 m sec^{-1}.

The profiles of the v-components of the wind (Figures 3-13 and 3-14) show very weak northward flow up to 40 km. Above this level it increases to 10 m sec^{-1} at 48 km for the location at 20°N in the winter and at 52 km in the summer. At 40°N however the winter wind increases to nearly 20 m sec^{-1} at 52 km while the summer wind never exceeds 7 m sec^{-1}. These stations are far enough southeast to escape the prevailing southward flow from the Arctic although the variability seen in the January 40°N data shows that it is often subject to the Arctic outbreaks.

The similarity of these profiles to those given in previous models (e.g. Groves, 1971) is highly encouraging, especially since the data was analyzed at fixed levels for all locations rather than by height for fixed locations. In fact checking of profiles on a more global basis shows a dependence of atmospheric parameters on height which is well in line with the works of previous authors. The only occasional problems found were with the wind profiles over data sparse regions or in areas and months of such extreme variability that statistical profiles were not very representative of actual profiles.

The final profiles used in the 4-D models were generated at 2 km levels from the statistics given at the five basic analysis levels. Linear interpolation was used for the standard deviation of all parameters and for the means of the temperature and wind components. Logarithmic interpolation was used for the mean pressure and density. The 4-D stratospheric model thus became a set of profiles at 5° latitude - longitude grid points from 0° longitude to 160°E longitude and from 0°N to 90°N. These profiles are stored on two magnetic tapes containing 12 files of one month each. For each month there are 739 records, each record containing 14 levels of the means and variances of pressure, temperature, density, and u and v wind components from 26 to 52 km. This model is not meant to be the ultimate stratospheric model because many more observations are needed to provide such a model. However, it does allow some evaluation of the basic characteristics of the stratosphere and the spatial and longitudinal variability found at these altitudes.
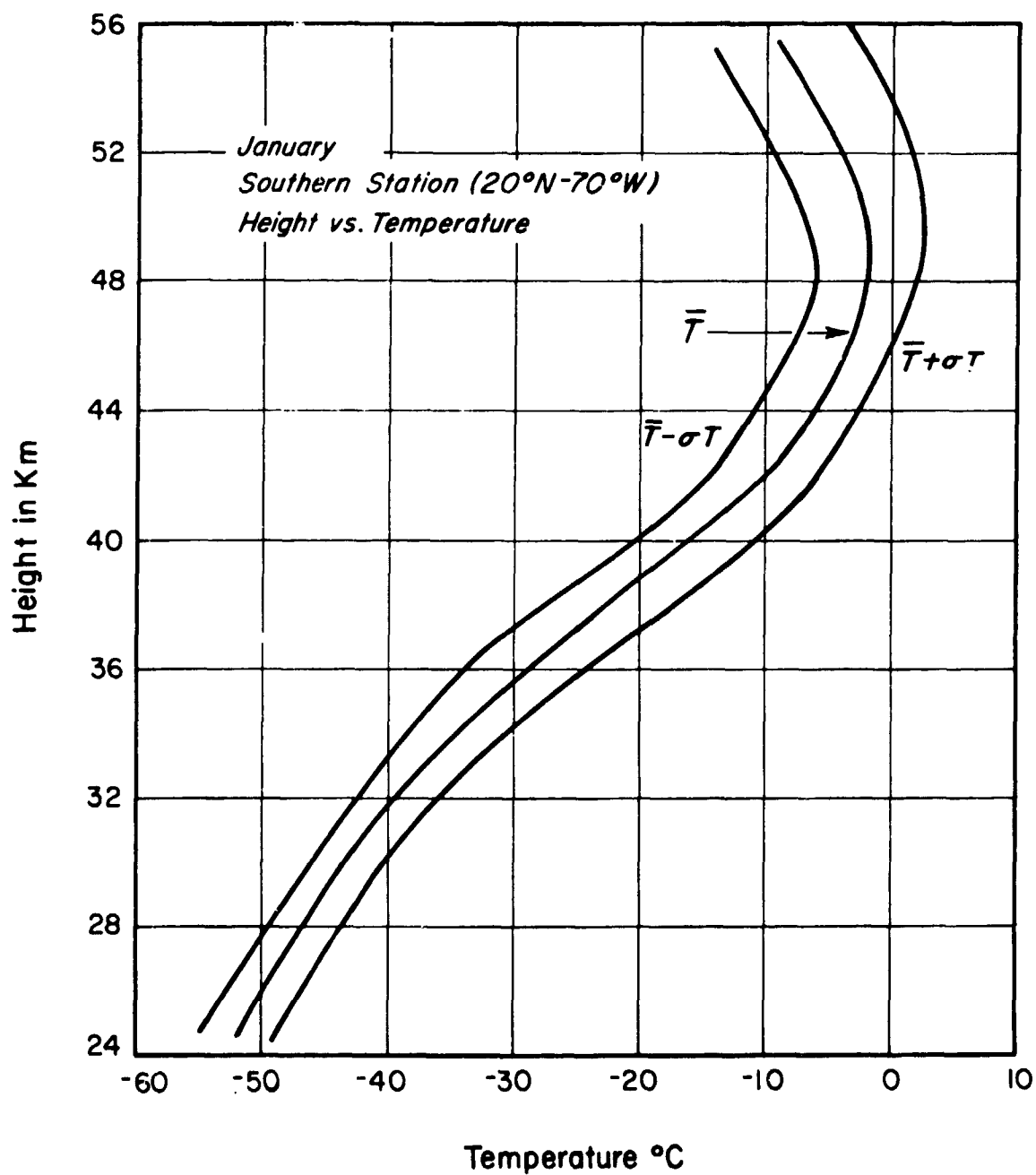
Figure 3-9a Stratospheric Temperature Profiles for January
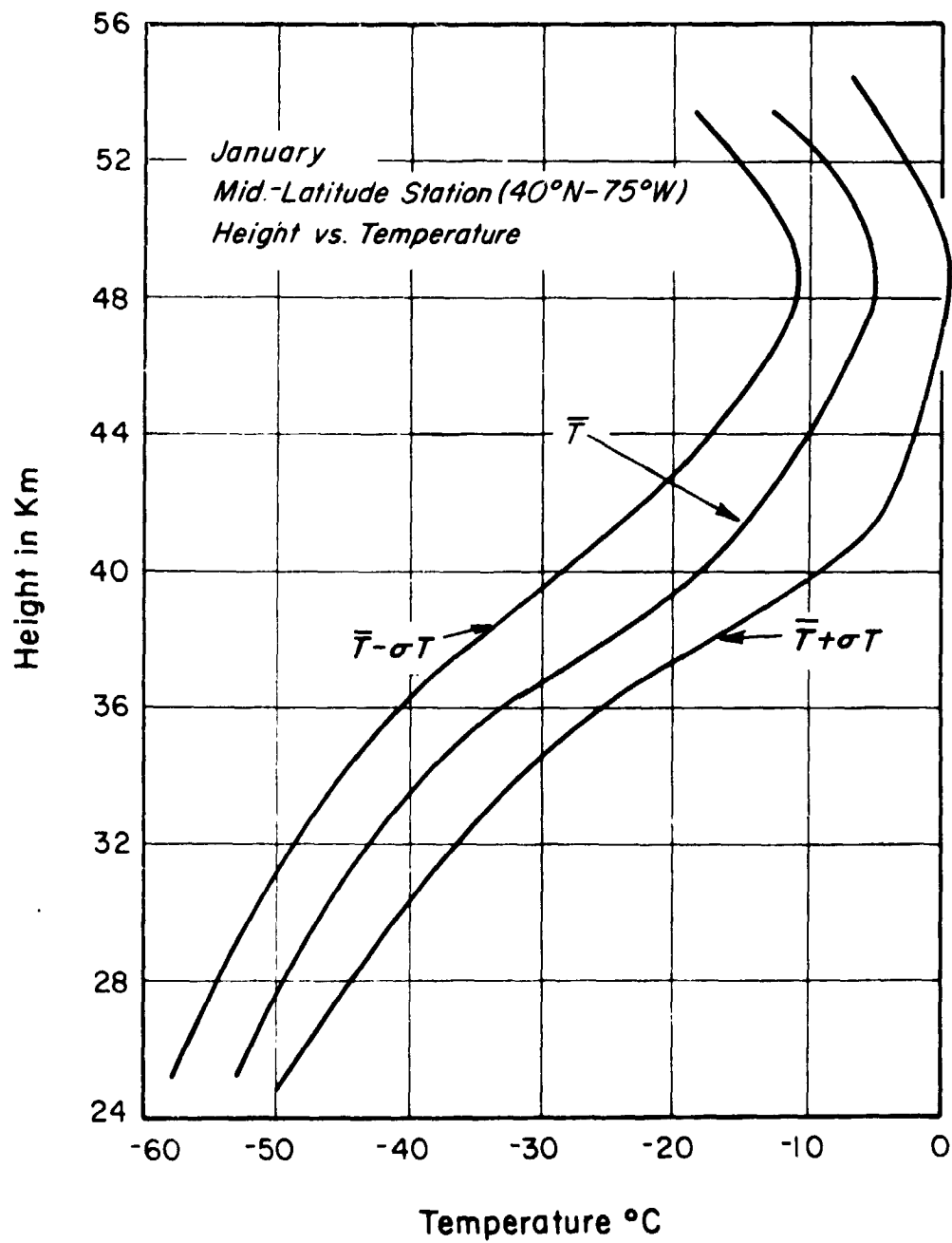
Figure 3-9b   Stratospheric Temperature Profiles for January
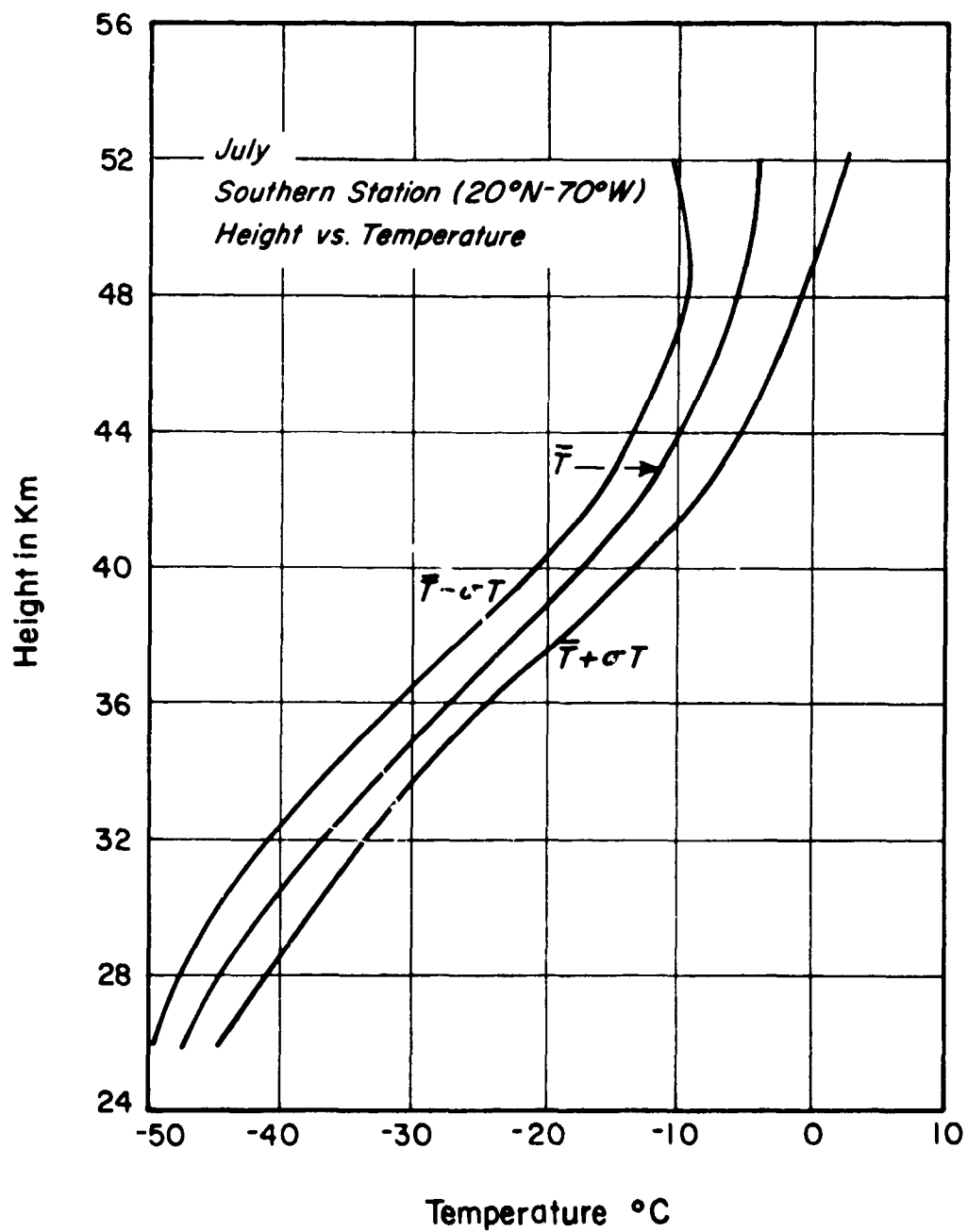
Figure 3-10a   Stratospheric Temperature Profiles for July
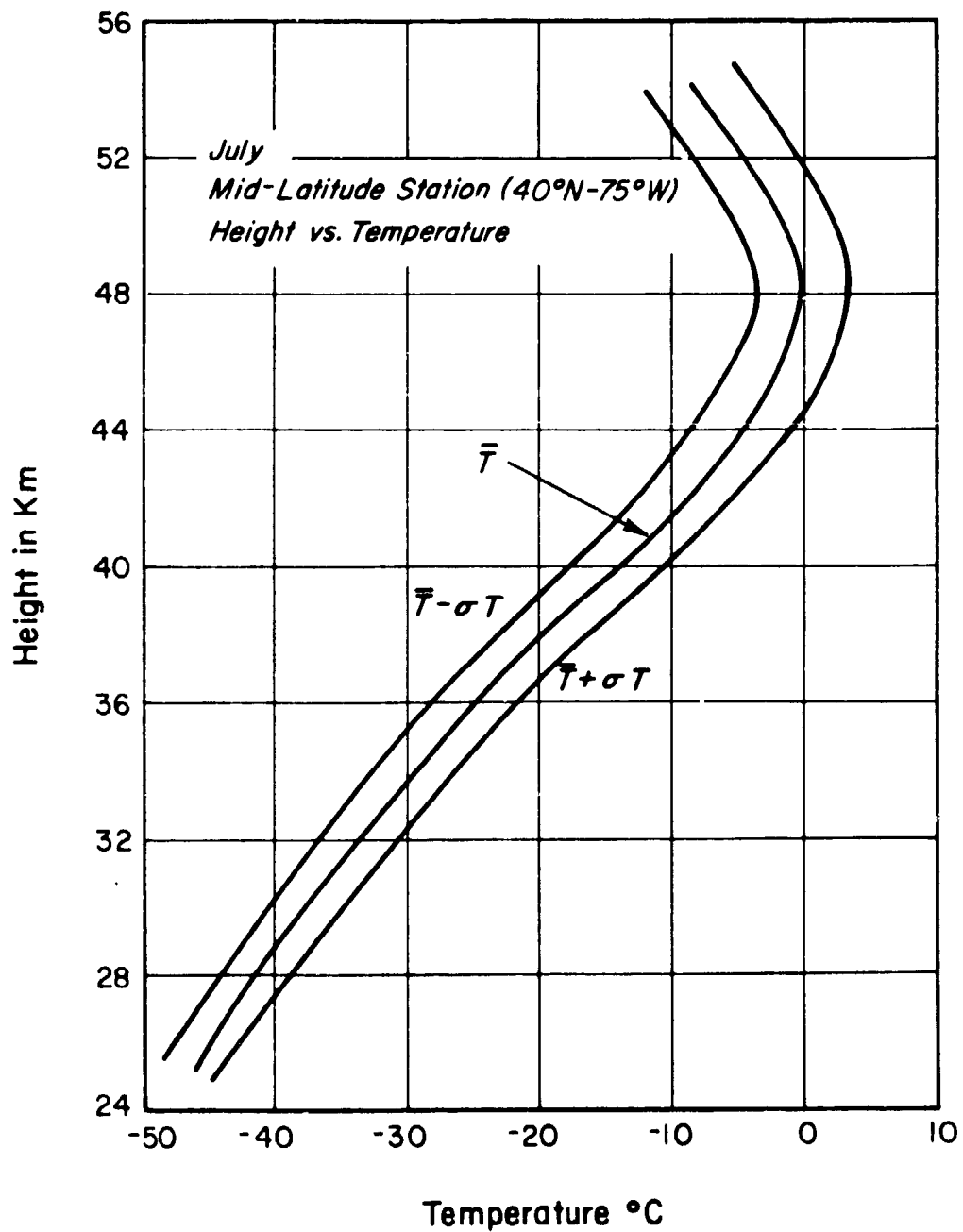
Figure 3-10b   Stratospheric Temperature Profiles for July
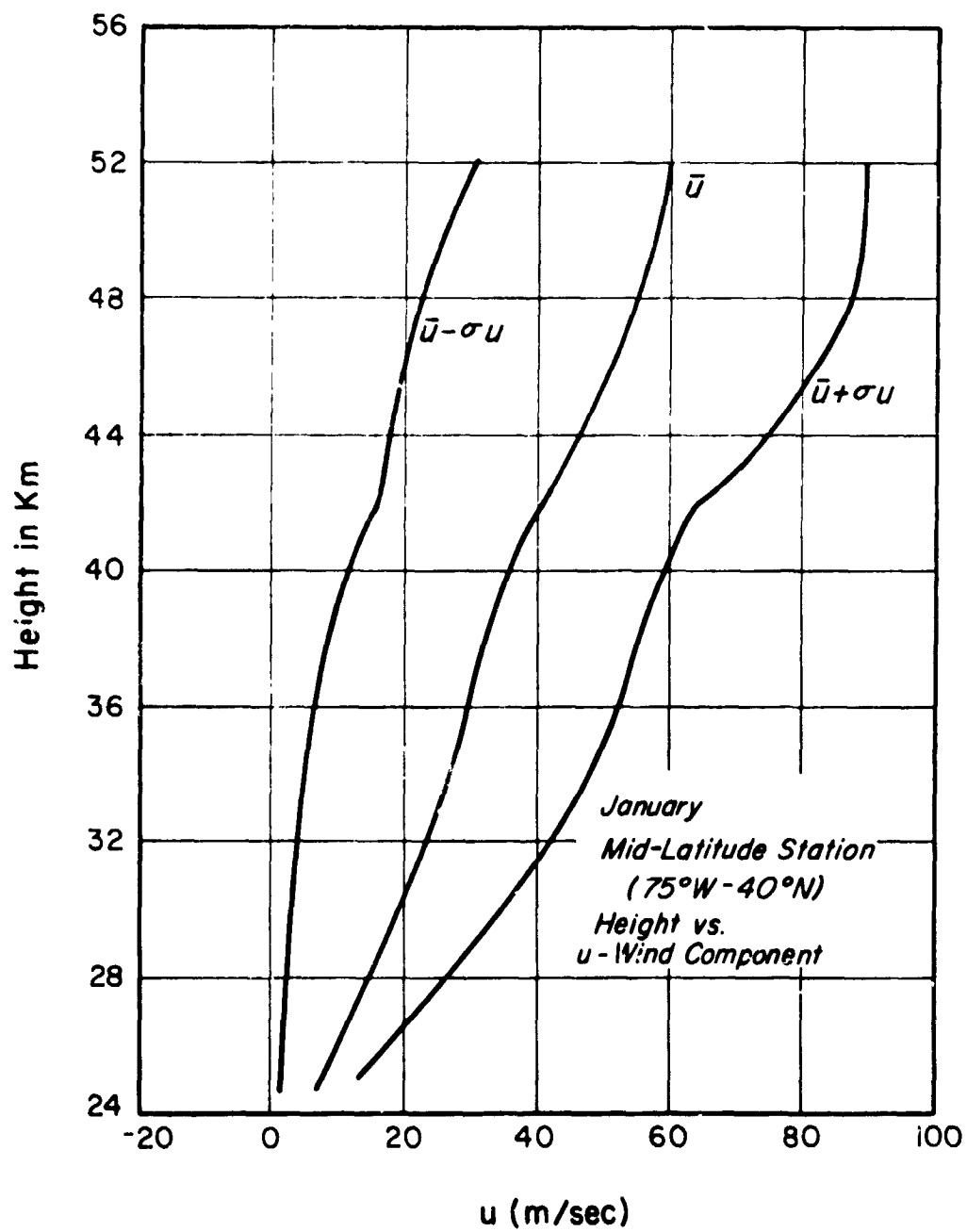
Figure 3-11a   Stratospheric West-East Wind Component Profiles
for January
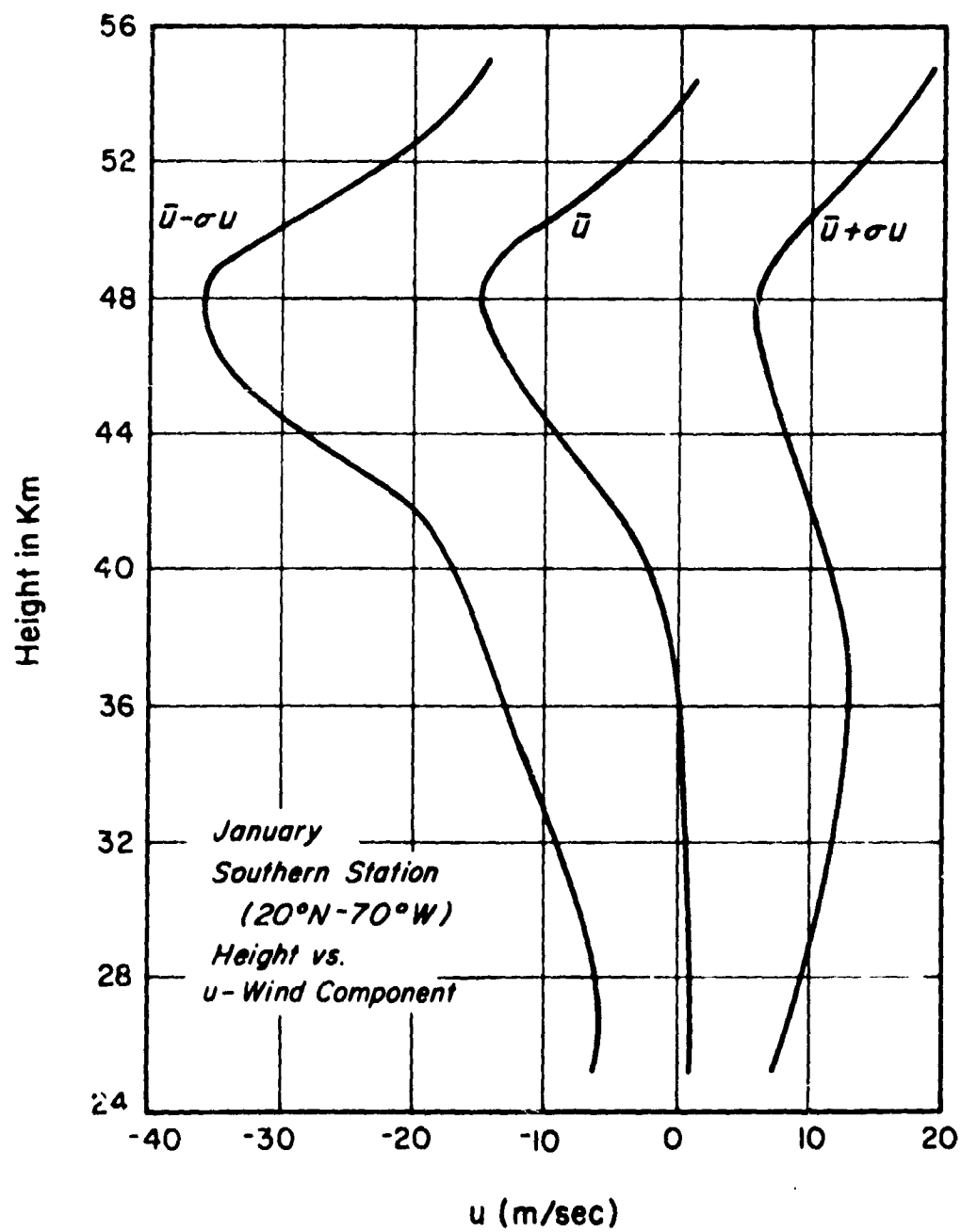
Figure 3-11b   Stratospheric West-East Wind Component Profiles
for January
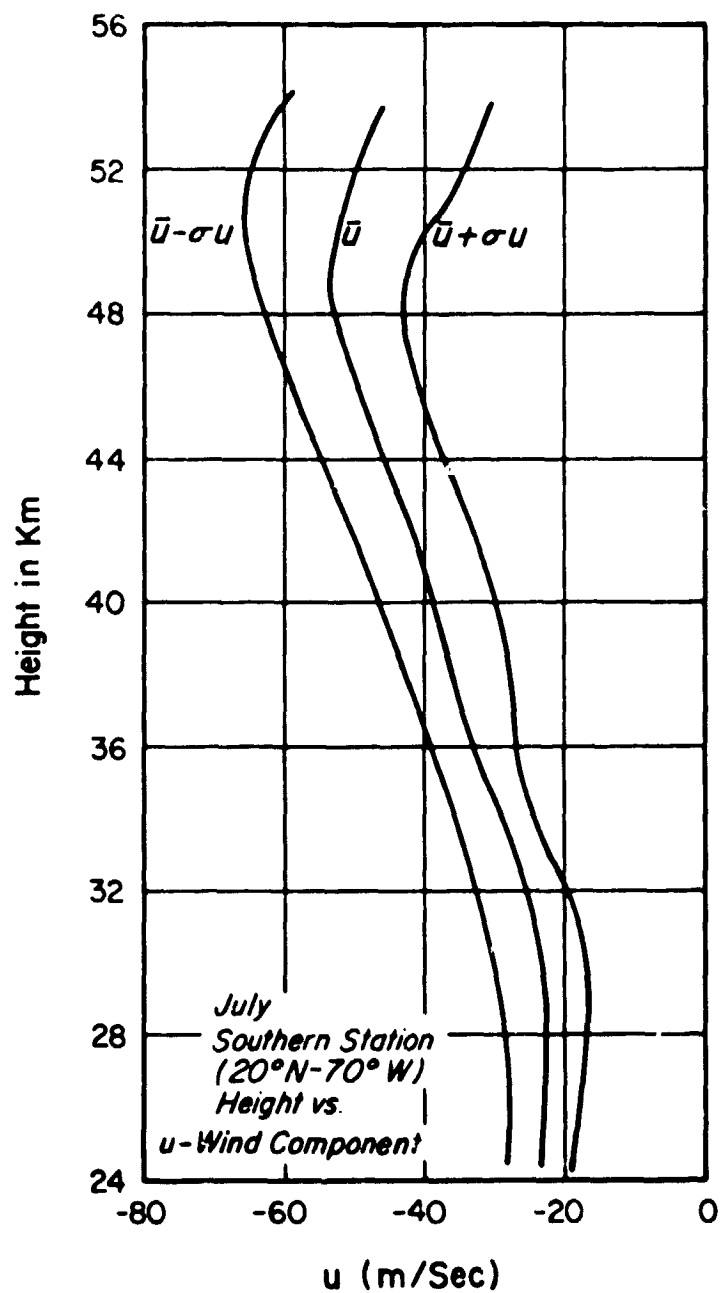
Figure 3-12a   Stratospheric West-East Wind Component Profiles
for July
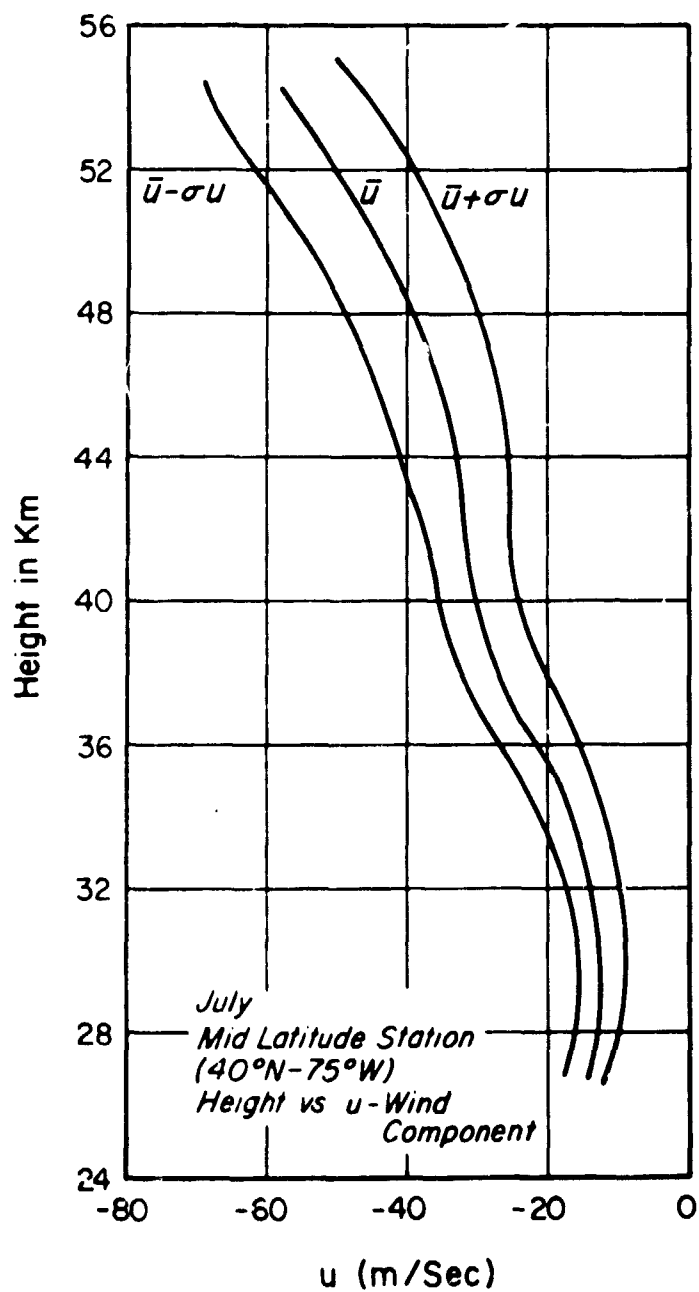
Figure 3-12b   Stratospheric West-East Wind Component Profiles
for July
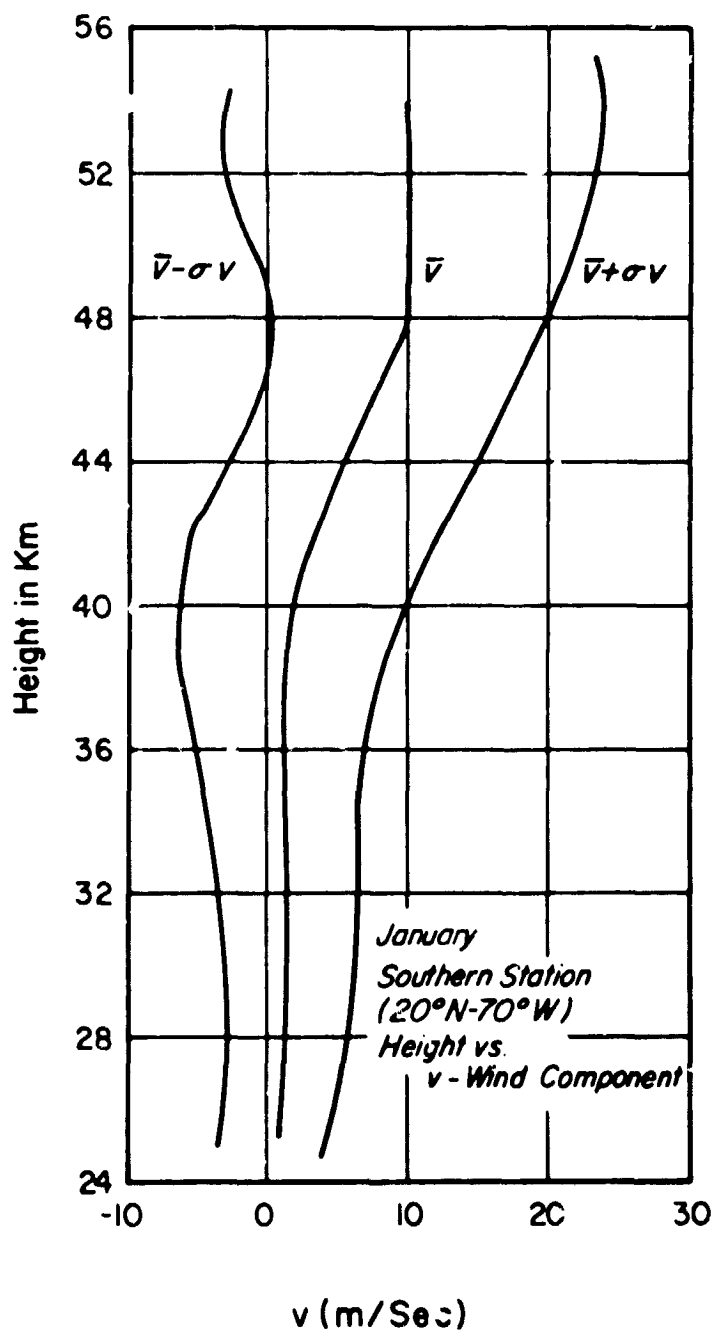
Figure 3-13a   Stratospheric South-North Wind Component Profiles for January

The figure shows a graph with "Height in Km" on the vertical axis (ranging from 24 to 56) and "v (m/Sec)" on the horizontal axis (ranging from -20 to 40). Three curves are labeled $\bar{v}-\sigma v$, $\bar{v}$, and $\bar{v}+\sigma v$.

January
Mid Latitude Station
(40°N-75°W)
Height vs.
v – Wind Components
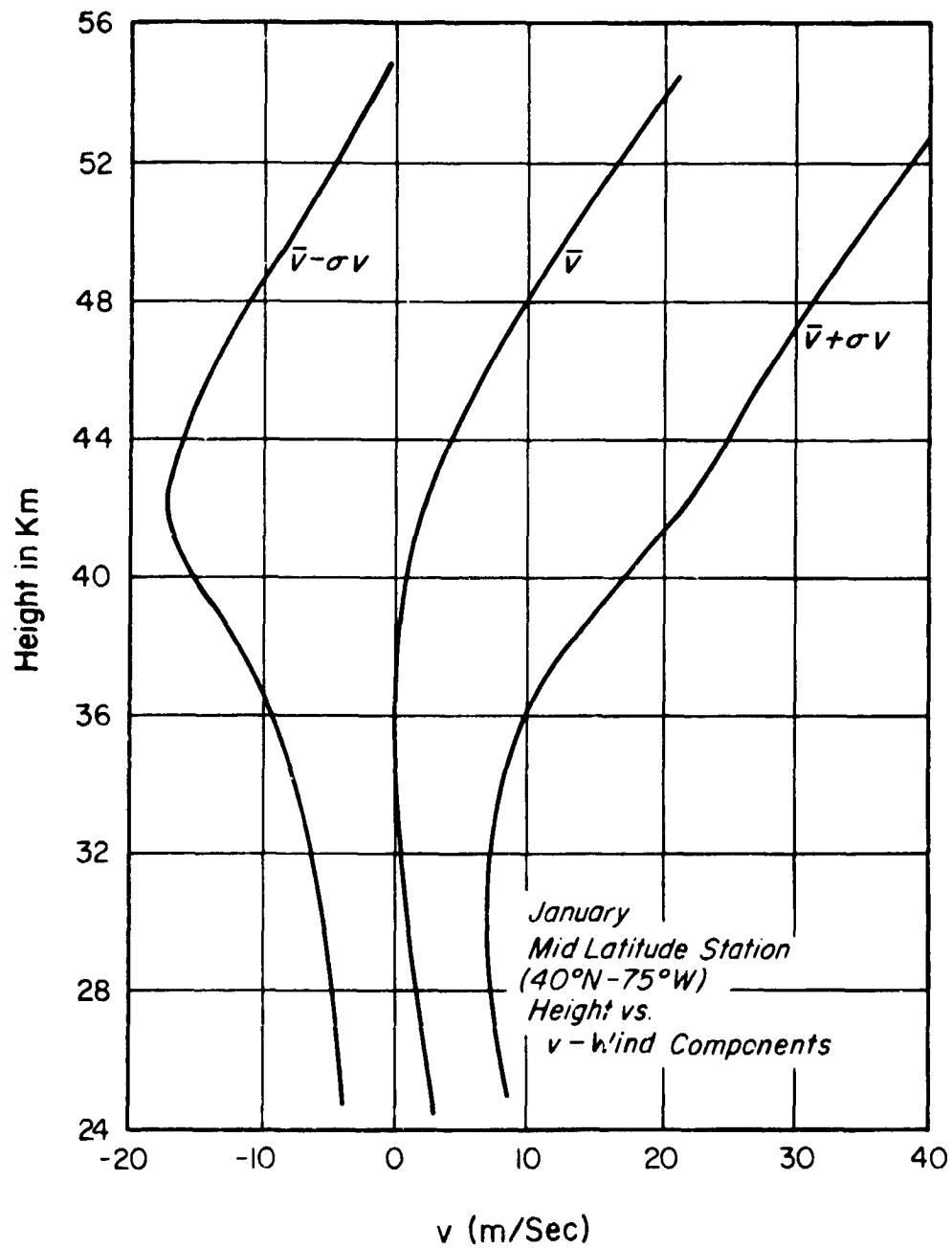
Figure 3-13b   Stratospheric South-North Wind Component Profiles
for January
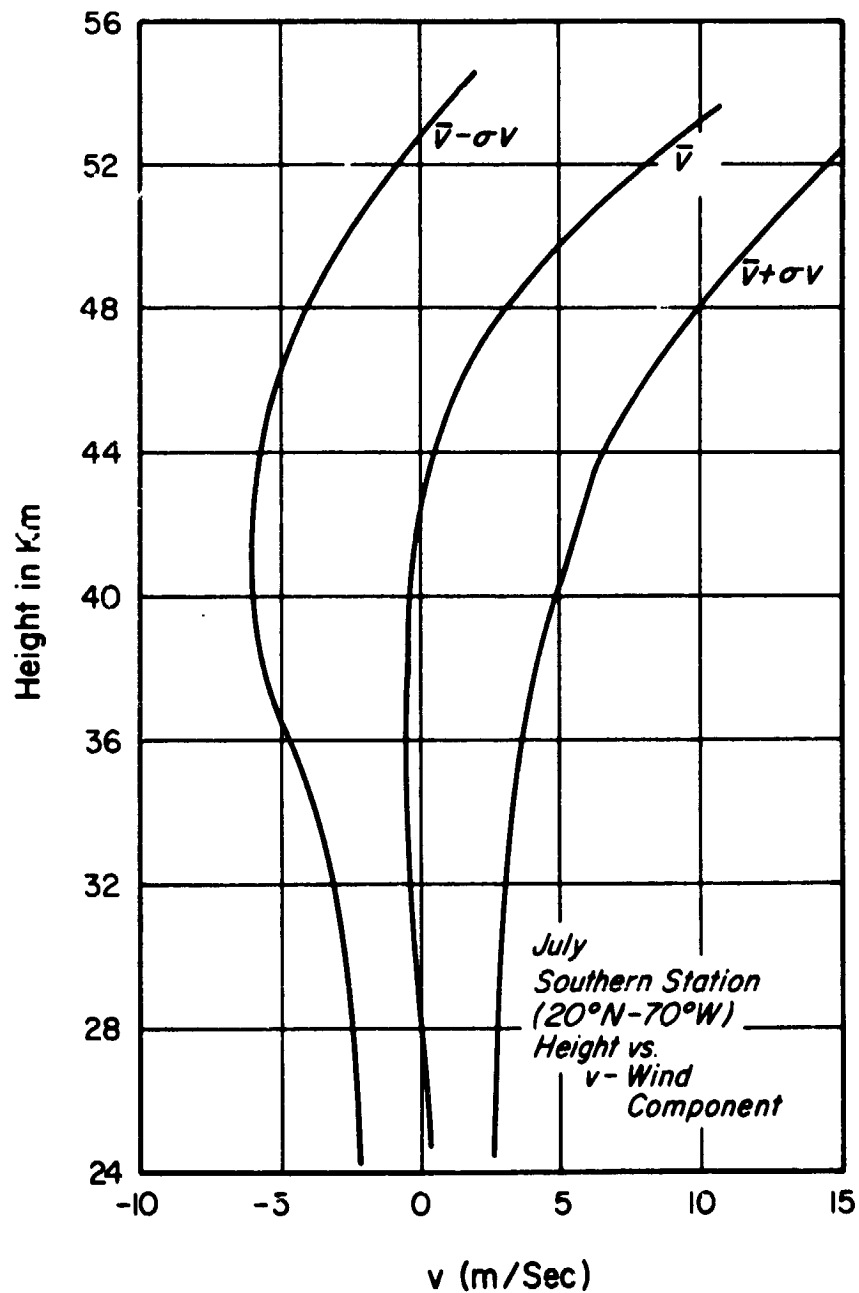
Figure 3-14a   Stratospheric South-North Wind Component
                Profiles for July
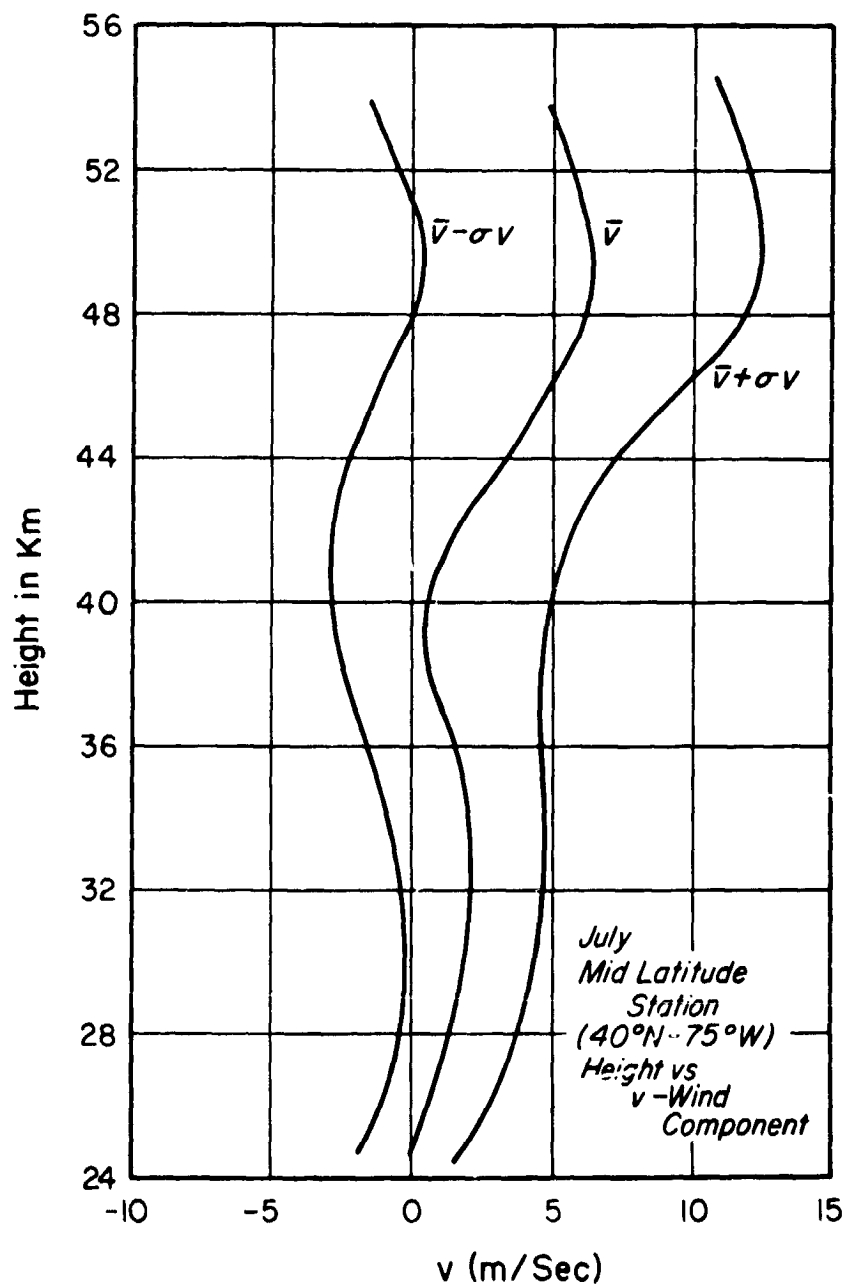
Figure 3-14b   Stratospheric South-North Wind Component Profiles
for July

4. THE 4-D WIND STATISTICS

The 4-D model developed by Spiegler and Fowler (1971) provided global statistics of the meteorological parameters of importance to remote sensing and radiometric studies. Hence the parameters selected for the model were those of pressure, temperature, water vapor and density, the atmospheric variables of the maximum importance in computing absorption and scattering at infrared, visible, and microwave wavelengths. The purpose of the current study, however, was the modification of the 4-D model to allow evaluation of other problems in the space program. The most important of these is the computation of vehicle trajectories for the planned space shuttle program, computations which require a knowledge of global winds and their spatial and temporal variability. To meet this requirement, the means and variances of the west-east and south-north wind components were computed globally at 1 km levels to be combined with the existing parameters in the 4-D model.

4.1 The Basic Data Set and Data Processing

Three primary data sets were used to derive the 4-D wind model:

> Four years of daily u and v wind components on the NMC grid supplied by NCAR for pressure levels from 850 to 100 mb, representing the daily analysis maps produced by the National Meteorological Center

> Mean monthly u and v wind components and heights at $5°$ latitude - longitude intersections for the Northern Hemisphere, for pressure levels from 1000 to 100 mb, supplied by NCAR

> and

> Mean monthly u and v wind components and heights at $5°$ latitude - longitude intersections for the Southern Hemisphere, for pressure levels from 1000 to 100 mb, supplied by NCAR.

These data sets, providing primarily geostrophic winds, were supplemented by radiosonde data contained in the MIT General Circulation Data Library and by the existing 4-D model, whose parameters permitted the computation of geostrophic winds.   PRECEDING PAGE BLANK NOT FILMED

From the first data set monthly means and variances of west-east (u) and south-north (v) wind components were computed for all points on the NMC grid. Latitudinal mean variances were also computed, at 5° intervals. Those for 20° N were used to supply the variances in the equatorial data set, and all latitudinal variances, with a six-month time switch, were used in the Southern Hemisphere. This approach was necessary to provide some guideline on zonal variability in areas where daily grid data was not available. In addition, the 850 mb grid point variances on the NMC grid were assumed to apply to the surface since no daily values were available there.

It was not possible to obtain wind data above 100 mb for any of the grids in use. Thus mean u and v wind components from 18 to 25 km were assumed to be geostrophic and were computed from the mean pressure and density given in the existing 4-D model. These computations used the formulae:

$$\bar{u}_i = \frac{-1}{\rho_i F} \left.\frac{\partial \bar{p}}{\partial y}\right|_i \tag{4-1}$$

$$\bar{v}_i = \frac{1}{\rho_i F} \left.\frac{\partial \bar{p}}{\partial x}\right|_i \tag{4-2}$$

where

$$\left.\frac{\partial p}{\partial x}\right|_i = \frac{(\bar{p}_0 - \bar{p}_2) + [(\bar{p}_1 - \bar{p}_3) - (\bar{p}_0 - \bar{p}_2)]\delta\phi}{(\lambda_2 - \lambda_1)\, Re \cos\phi}$$

$$\left.\frac{\partial p}{\partial y}\right|_i = \frac{(\bar{p}_1 - \bar{p}_0) + [(\bar{p}_3 - \bar{p}_2) - (\bar{p}_1 - \bar{p}_0)]\delta\lambda}{(\theta_2 - \theta_1)\, Re}$$

and

$$\delta\phi = (\phi_i - \phi_1)/(\phi_2 - \phi_1)$$

$$\delta\lambda = (\lambda_i - \lambda_1)/(\lambda_2 - \lambda_1)$$

where

ϕ = latitude

λ = longitude

$\bar{p}_k$ = mean pressure at point k

ρ_i = mean density at point i

F = Coriolis parameter

  = $2\,\Omega \sin\phi$

54

$\bar{u}_i$ = mean eastward wind component

$\bar{v}_i$ = mean northward wind component

Re = radius of the earth

The subscripts correspond to those shown in Figure 4-1, with the differences in latitude and longitude always corresponding to 10°. This meant the direct use of values on the Southern Hemisphere grids but involved the conversion of the NMC grid to a 5° latitude-longitude grid prior to the computation of the winds.

The winds in the Northern Hemisphere equatorial grid, however, were not computed geostropically for the primary reason that discontinuities appeared in the pressure and density values near 20° N. These discontinuities are apparently caused by the extrapolation of values over the equator during the original development of the 4-D model which, while providing realistic values, did not provide values in precise agreement with those generated by real data for the NMC grid. Better agreement is found with values generated by the curve-fit coefficients, but it was still difficult to derive realistic winds for this region. Hence the following approach was used.

Monthly means and variances of u and v wind components were computed for the 50, 30 and 10 mb levels for all stations reporting data in the MIT General Circulation Data Library. This data set, containing 5 years of daily radiosonde measurements at 704 stations in the Northern Hemisphere, can be analyzed to provide grid wind statistics in the troposphere. However, at 50 mb and greater altitudes, the number of observations is quite limited, making such a spatial analysis difficult. So station statistics computed for these levels were averaged to generat mean latitudinal wind means and variances for 5° bands from the equator to the pole.

These latitudinal values were used for two purposes. First, for the equatorial grid, the monthly means and variances were utilized to provide all of the upper level wind statistics, replacing the need for the geostrophic computation of the means. Second, for NMC and Southern Hemisphere grids, the mean latitudinal variances were used, in conjunction with the geostrophic means for each grid point, to provide the wind data from 18 to 25 km. For the Southern Hemisphere, of course, a six-month time switch was assumed in incorporating the variances. These variances
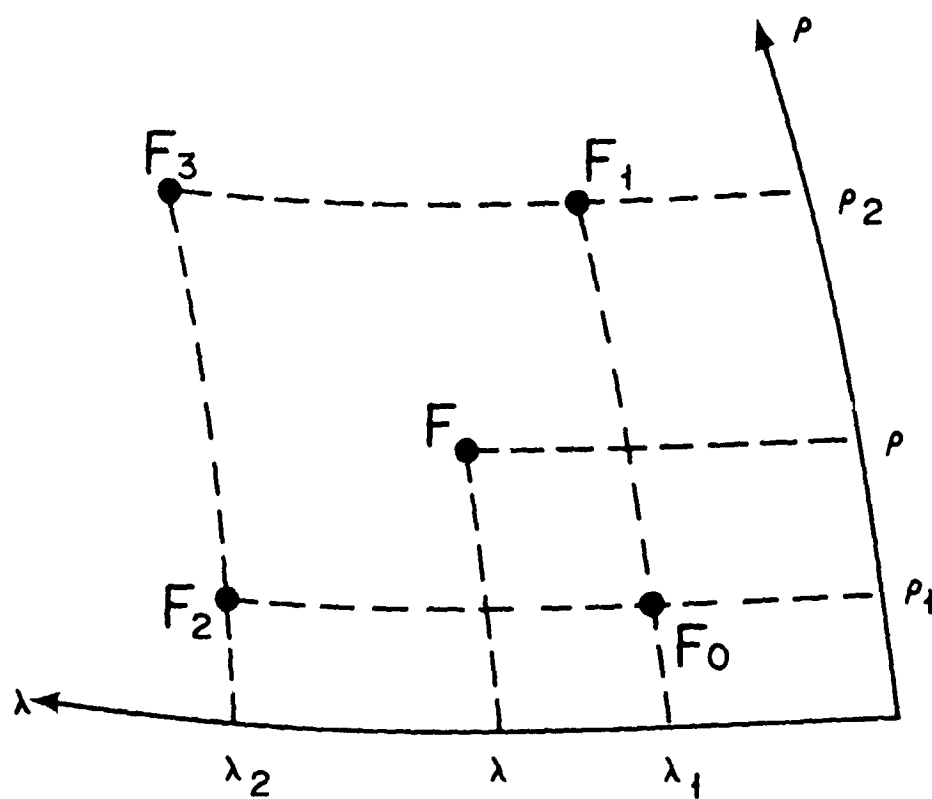
Figure 4-1   Two Dimensional Interpolation of Parameter F as a
Function of latitude φ and West Longitude λ

probably overestimate those found in the Southern Hemisphere where the wind flow is much less perturbed but do permit an estimate of the variability and provide an upper limit on expected changes.

The pressure level data sets generated by these computations are summarized in Table 4-1. All of these levels were then combined vertically to produce one set of data for each of the three grids, and constant height values were computed using the following linear interpolation scheme:

$$X_{km} = X_{p_1} + (X_{p_2} - X_{p_1}) (Z_{km} - Z_{p_1})/(Z_{p_2} - Z_{p_1}) \qquad (4-3)$$

where

X is the parameter to be interpolated $\overline{U}$, $\overline{V}$, $\sigma\overline{U}$, $\sigma\overline{V}$

km is the kilometer level desired

p_1 is the pressure level just below the kilometer level

p_2 is the pressure level just above the kilometer level

Z_{p_i} is the mean height of pressure level i

Z_{km} is the height of the desired kilometer level

For these computations, the mean height for each pressure level was assumed to be that contained on the 5° latitude - longitude Northern and Southern Hemisphere tape. This height was converted to the NMC grid for interpolation there; otherwise it was used as given on tape. For the surface level, the actual grid point heights used in the previous study were applied here.

Two tapes were generated as a final product of this processing with each tape record containing means and variances of the U and V wind components from the surface to 25 km at one km levels for each grid point. The format follows that for the original 4-D data set with a file for each month containing 288 records for the equatorial grid, 1977 records for the NMC grid and 1225 records for the Southern Hemisphere grid. These records thus can be easily used in conjunction with those in the original 4-D model to generate combined profiles of pressure, temperature, water vapor, density and winds. Or they can be used alone to show the wind structure over any point on the earth's surface

TABLE 4-1

Level	NMC Grid		Equatorial Grid		Southern Hemisphere Grid	
	Mean	Variance	Mean	Variance	Mean	Variance
Surface	5° L-L Tape 1	850 mb grid values	5° L-L Tape 1	850 mb values	5° L-L Tape 2	850 mb values
850 mb	Computed from daily NMC wind grids		"	20° Latitudinal Mean Variances from NMC grid	"	Mean Latitudinal Variances from NMC grid (six month time switch)
700 mb		"	"	"	"	"
500 mb		"	"	"	"	"
300 mb		"	"	"	"	"
200 mb		"	"	"	"	"
100 mb		"	"	"	"	"
50 mb	Geostrophic winds from 4-D model	Mean Latitudinal Variances from Station Data	Latitudinal Means & Variances from Station Data		Geostrophic Winds from 4-D Model	Mean Latitudinal Variances from Station Data (six month time switch)
30 mb	"	"		"	"	"
10 mb	"	"		"	"	"

58

4.2 The Verification of the Global Wind Statistics

The derivation of the wind profiles of necessity involved many assumptions about the continuity and consistency of the various data sets. Thus a great deal of comparison and checking went into the various phases of the computation to insure the accuracy of the results. The geostrophically computed wind statistics for the NMC grid were compared with the radiosonde station statistics derived from the General Circulation Data Library for levels above 100 mb. The means of both the u and v wind components showed excellent correlation in the point by point comparison and validated the assumption that the detailed features of the high level wind fields could be accurately derived from the features of the pressure and density fields. No such comparison could be made for the Southern Hemisphere, unfortunately, due to a lack of data at the high levels, but the general flow patterns and winds speeds derived geostrophically appear reasonable.

Verification was also performed on the wind data computed for the troposphere. The 500 mb means and standard deviations computed for the NMC grid from the daily wind values were carefully scrutinized in comparison with the same parameter given by Lahey et al (1958). These latter statistics derived from grid data for 1947 through 1953 showed remarkable agreement with the values derived here from the 1969-1972 data set both in the location of maximum and minimum wind means and standard deviations, and in the values given for these statistics at selected locations. Further support of the reliability of our wind statistics was provided by the vertical-longitudinal cross sections given for selected latitudes by Newell et al (1972) and by the mean latitudinal wind values given for the equatorial region by Oort and Rasmusson (1971). Finally reference to other wind field analyses such as those provided by the NAVAIR 50-1C-51 and 50-1C-52 documents and by Heastie and Stephenson (1960) completed the verification of the accuracy of the global wind statistics with a strong belief in the grid point profiles of wind components.

4.3 The 4-D Wind Profiles

Figures 4-2 through 4-7 show the computed January and July wind statistics for three points on the NMC grid. These points are located near 40° N, 135° W (point 601) near 75° N, 80° W (point 801) and near 18° N, 60° E (point 1801) and display the characteristics of the wind flow typical of their locations. The January winds are dominated by strong westerly flow near 40° N, with a slight northerly component indicating the intrusion of arctic air at the lower and upper levels of the atmosphere. The maximum winds occur in the 10-12 km region where they show little south-north component and reflect the predominance of a westerly jet. Frequent changes in the direction and intensity of this jet, however, are clearly seen in the large standard deviations (18-20 m sec^{-1}) found for both wind components at these levels.

In contrast to this variability the winter statistics for 20° N show a much more stable flow pattern with standard deviations less than 10 m sec^{-1} for most levels of the atmosphere. Again westerly flow dominates except near the surface and above 23 km where the flow is easterly. However the south-north component changes direction in the vertical with the lower troposphere characterized by the winds from the north and higher levels showing weak compensatory flow to the north.

The January data at 75° N, 80° W is characterized primarily by weak flow from the southwest through most of the troposphere with north-easterly flow at the surface and northwesterly flow in the stratosphere. This flow is part of the circulation around an arctic low located near this area in the lower troposphere, and moving farther to the east with altitude to form one major low at 90° E at 18 km.

The July wind data contrasts sharply with the January statistics. The midlatitude westerlies are much weaker and less variable with flow from the south dominating at altitudes above 5 km. The northerly flow found in the surface layers is caused by the dominance of this location by a shallow Pacific high. This circulation disappears from the area around 500 mb (5-6 km) leaving the zone in the path of the westerlies circling the globe. Above 20 km, however, the circulation shifts to the easterly flow which characterizes the stratosphere during the summer months.

NMC GPID POINT NO. 601   MONTH 1

LEVEL	U	VARIANCE	V	VARIANCE
SFC	7.41	91.10	.89	92.88
1 KM	7.54	91.10	-.08	92.88
2 KM	8.78	108.25	-.49	114.20
3 KM	11.05	126.88	-.39	137.71
4 KM	13.14	151.38	-.65	170.24
5 KM	15.22	178.25	-.93	206.53
6 KM	17.29	209.84	-.98	244.42
7 KM	19.34	248.95	-.68	282.25
8 KM	21.40	290.10	-.38	322.81
9 KM	23.45	335.10	-.08	366.08
10 KM	24.15	337.05	.06	363.06
11 KM	24.44	325.31	.14	345.65
12 KM	24.42	306.47	.14	321.99
13 KM	22.71	250.60	-.40	264.85
14 KM	21.00	200.35	-.93	213.29
15 KM	19.30	155.72	-1.47	167.30
16 KM	17.59	116.70	-2.00	126.90
17 KM	14.96	112.75	-2.34	105.25
18 KM	12.33	108.86	-2.68	85.62
19 KM	10.44	105.03	-3.03	68.02
20 KM	8.55	101.28	-3.39	52.44
21 KM	6.66	124.00	-3.74	56.30
22 KM	4.77	149.02	-4.10	60.31
23 KM	2.88	176.34	-4.45	64.45
24 KM	.99	213.89	-4.81	71.22
25 KM	-.90	269.73	-5.16	82.75

Figure 4-2   4-D Wind Statistics for January at 40°N, 135°W

(wind speed in m/s)

NMC GRID POINT NO.   801   MONTH   1

LEVEL	U	VARIANCE	V	VARIANCE
SFC	-1.67	16.94	-2.44	35.98
1 KM	-.56	16.94	-1.68	35.98
2 KM	.09	30.98	-.73	43.61
3 KM	.53	49.47	.21	54.39
4 KM	.85	72.00	1.00	72.12
5 KM	1.16	100.87	1.78	92.35
6 KM	1.25	120.30	2.33	105.09
7 KM	1.33	140.81	2.86	118.19
8 KM	1.40	162.92	3.39	132.04
9 KM	1.38	155.47	3.32	119.95
10 KM	1.30	131.91	2.91	94.58
11 KM	1.25	111.46	2.49	73.54
12 KM	1.60	115.05	2.07	76.72
13 KM	1.95	118.70	1.65	79.96
14 KM	2.30	122.41	1.23	83.27
15 KM	2.65	126.18	.81	86.65
16 KM	5.13	111.26	-.57	112.46
17 KM	7.62	97.29	-1.94	141.63
18 KM	10.10	84.25	-3.32	174.16
19 KM	11.42	72.15	-4.66	210.04
20 KM	12.74	60.09	-6.00	249.29
21 KM	14.06	95.07	-7.34	307.17
22 KM	15.38	136.68	-8.68	371.08
23 KM	16.70	185.83	-10.02	441.03
24 KM	18.01	202.92	-11.36	480.75
25 KM	19.33	220.18	-12.70	521.65

Figure 4-3   4-D Wind Statistics for January at 75°N, 80°W

(wind speed in m/s)

NMC GRID POINT NO. 1801   MONTH 1

LEVEL	U	VARIANCE	V	VARIANCE
SFC	-5.90	52.77	-4.63	13.09
1 KM	-.81	52.77	-3.07	13.09
2 KM	1.86	52.77	-2.26	13.09
3 KM	1.86	52.77	-2.24	13.00
4 KM	4.38	52.38	-2.21	15.75
5 KM	7.37	51.02	-2.15	19.20
6 KM	10.27	52.98	-2.10	23.03
7 KM	12.68	64.01	-2.08	27.38
8 KM	15.10	76.10	-2.07	32.11
9 KM	17.51	89.22	-2.06	37.21
10 KM	19.80	99.41	-1.86	43.69
11 KM	21.88	102.31	-1.33	52.77
12 KM	23.96	105.26	-.79	62.71
13 KM	24.27	97.06	-.37	63.11
14 KM	23.39	82.38	-.01	57.01
15 KM	22.51	68.90	.35	51.21
16 KM	21.63	56.62	.71	45.73
17 KM	13.56	52.22	.24	34.82
18 KM	5.49	47.99	-.22	25.41
19 KM	4.43	43.94	.12	17.47
20 KM	3.38	40.07	.46	11.01
21 KM	2.32	57.33	.80	12.47
22 KM	1.26	77.67	1.14	14.02
23 KM	.21	101.09	1.48	15.66
24 KM	-.95	121.21	1.82	17.31
25 KM	-.91	125.38	2.16	18.83

Figure 4-4   4-D Wind Statistics for January at 18°N, 60°E

(wind speed in m/s)

NMC GRID POINT NO.   691   MONTH 7

LEVEL	U	VARIANCE	V	VARIANCE
SFC	.33	25.81	-3.68	30.73
1 KM	2.41	25.81	-2.42	30.73
2 KM	4.49	42.27	-1.36	37.46
3 KM	6.38	62.77	-.57	44.86
4 KM	7.54	80.85	-.16	52.64
5 KM	8.67	100.08	.19	60.99
6 KM	9.75	119.09	.58	71.03
7 KM	10.64	130.59	1.14	86.68
8 KM	11.52	142.62	1.71	103.90
9 KM	12.41	155.17	2.27	122.67
10 KM	13.02	165.24	2.85	134.26
11 KM	13.34	172.32	3.45	136.93
12 KM	13.65	179.54	4.04	139.61
13 KM	12.25	142.52	4.02	108.74
14 KM	10.48	102.19	3.87	76.05
15 KM	8.72	68.55	3.71	49.20
16 KM	6.95	41.61	3.56	28.17
17 KM	4.42	33.57	2.89	21.67
18 KM	1.99	26.39	2.73	16.02
19 KM	.61	20.07	2.15	11.23
20 KM	-.67	14.61	2.08	7.28
21 KM	-1.96	13.95	2.01	6.54
22 KM	-3.24	13.30	1.93	5.84
23 KM	-4.53	12.67	1.86	5.18
24 KM	-5.81	12.05	1.78	4.55
25 KM	-7.10	11.85	1.71	4.53

Figure 4-5   4-D Wind Statistics for July at 40°N, 135°W

(wind speed in m/s)

NMC GRID POINT NO. 801   MONTH 7

LEVEL	U	VARIANCE	V	VARIANCE
SFC	-1.01	18.24	-1.28	15.54
1 KM	-.67	18.24	-.28	15.54
2 KM	-.23	27.57	.24	19.30
3 KM	.27	38.99	.43	23.69
4 KM	.54	55.22	.59	32.35
5 KM	.81	74.26	.76	42.37
6 KM	1.09	94.48	.79	55.06
7 KM	1.38	115.43	.71	70.82
8 KM	1.66	138.47	.63	88.56
9 KM	1.94	163.61	.54	108.28
10 KM	1.51	117.76	.42	79.03
11 KM	1.06	78.26	.29	53.54
12 KM	.65	51.33	.17	35.69
13 KM	.32	39.83	.06	27.21
14 KM	-.01	29.79	-.06	19.87
15 KM	-.34	21.20	-.18	13.69
16 KM	-.67	14.07	-.30	8.65
17 KM	-1.18	11.81	-.38	7.55
18 KM	-1.69	9.74	-.47	6.51
19 KM	-2.17	7.87	-.27	5.56
20 KM	-2.65	6.29	-.07	4.69
21 KM	-3.13	5.71	.13	4.53
22 KM	-3.62	5.23	.33	4.39
23 KM	-4.10	4.78	.53	4.25
24 KM	-4.58	4.34	.74	4.11
25 KM	-5.06	4.24	.94	4.17

Figure 4-6   4-D Wind Statistics for July at 75°N, 80°W

(wind speed in m/s)

LEVEL	U	VARIANCE	V	VARIANCE
SFC	14.39	86.81	5.28	35.29
1 KM	7.03	86.81	2.23	35.29
2 KM	3.52	68.87	-.02	25.09
3 KM	3.05	53.01	-1.65	16.62
4 KM	4.07	46.43	-2.28	16.26
5 KM	5.29	41.23	-2.78	16.87
6 KM	6.09	37.57	-3.26	18.37
7 KM	4.46	41.18	-3.67	25.62
8 KM	2.83	44.95	-4.08	34.07
9 KM	1.24	48.89	-4.50	43.72
10 KM	-1.67	52.45	-4.83	54.06
11 KM	-7.38	54.88	-4.98	64.25
12 KM	-13.08	57.37	-5.14	75.32
13 KM	-17.03	55.61	-4.95	78.33
14 KM	-19.31	50.02	-4.44	73.24
15 KM	-21.59	44.72	-3.93	68.32
16 KM	-23.88	39.72	-3.42	63.58
17 KM	-20.99	34.38	-.99	48.06
18 KM	-18.10	29.42	1.44	34.71
19 KM	-19.15	24.85	1.60	23.53
20 KM	-20.26	20.66	1.77	14.52
21 KM	-21.26	32.32	1.93	14.32
22 KM	-22.31	46.59	2.09	14.13
23 KM	-23.36	63.45	2.25	13.94
24 KM	-24.41	82.76	2.41	13.74
25 KM	-25.46	100.85	2.57	13.37

Figure 4-7   4-D Wind Statistics for July at 18°N, 60°E

(wind speed in m/s)

Easterly flow is also seen in the upper levels of both the 75° N location and the 20° N location although the total vertical profiles differ significantly. Again the winds at 75° N, 80° W are very weak and their changes through the troposphere are associated with the position and intensity of the Arctic low at different altitudes. As the stratosphere is entered the wind direction shifts, reflecting the differences in circulation patterns between the troposphere and the stratosphere.

Localized circulation also is visible in the 20° N statistics where the lower troposphere is dominated by a cyclone which gives way to an anticyclone in the upper troposphere. Very strong easterlies are found above 20 km supporting the July stratospheric wind maximum found near this latitude in the previous section.

Comparison of these profiles with vertical cross sections provided for the same locations by Newell et al (1972), Crutcher and Meserve (1970) and Belmont et al (1975), and study of other profiles now included in the 4-D model have clearly shown that a very strong capability is now available for the simulation of atmospheric conditions. Means and variances of the u and v wind components are now readily available for 3490 grid points spanning the globe with these statistics provided at 1 km levels from the surface to 25 km. Alone they permit an excellent evaluation of the earth's circulation; in conjunction with the previously developed 4-D model they specify all major parameters of the earth's atmosphere.

5. CONCLUSIONS AND RECOMMENDATIONS

5.1 Summary

The previous sections have presented the results of the modifications to the 4-D atmospheric model and the cloud data bank. These will be summarized here.

5.1.1 The Results of the Cloud Cover Analysis

Comparison of the LANDSAT observed cloud cover with observations made from the ground showed very good agreement for the 1/2° field of view, except in cases of less than 20% coverage where the satellite overestimates, and in cases of greater than 80% coverage where the satellite underestimates. (For intermediate ranges, the satellite underestimates very slightly.) In general, simulation of satellite viewed cloud cover using ground observed data should provide excellent results with a 10% error appearing only for clear and completely overcast conditions. For a 1/4° field of view, however, the satellite sees about 5% less cloudiness for all coverage greater than 20%; simulation of this field of view should show an appropriate reduction in cloud cover.

The effects of cloud shadow on total obscuration do not seem to be severe except for elevation angles of less than 30° and cloud coverage between 20 and 50%. In general, cloud shadows add about 5% to the total coverage so that on a statistical basis it improves the correlation between satellite and surface observations, and permits good simulation of ground obscuration using surface sky measurements. Simulation of only low elevation angles, however, should carefully evaluate the cloud shadow effect for it can be very significant under certain cloud conditions.

5.1.2 The Stratospheric Model

The rocketsonde measurements made by the Meteorological Rocket Network between 1961 and 1972 provided statistics of pressure, density, temperature and winds in the stratosphere which permitted the derivation of a limited grid model between 26 and 52 km altitude. This grid contains means and variances of the above parameters at 5° latitude -

longitude intersections from the Greenwich Meridian west to 160° E and from the equator to 90° N. The derived results show good agreement with previous studies of the stratosphere despite the need for some subjective analysis over data sparse areas and the lack of consistent periods of record for the stations used. Thus it is felt that the model developed here provides a good first-cut representation of the spatial and temporal variations in the stratosphere and permits an evaluation of expected atmospheric changes along a vehicle re-entry trajectory.

5.1.3 The 4-D Wind Model

Global means and variances of the east-west and north-south wind components were derived at 1 km levels from the surface to 25 km. These winds complete the basic 4-D model in its treatment of all atmospheric parameters and thus generalizes its application to aspects of space missions not related to radiometric studies. Derived from the same basic data sets used in the original 4-D model, the winds show the same global characteristics and can be used either alone or in conjunction with the other parameters.

5.2 Recommendations

The results presented above represent a tremendous increase in the utility and applications of the 4-D model and further study of the applicability of the cloud bank. However, additional research in the following areas is recommended to refine the above results, research that was not possible under the temporal and fiscal limitations of this study.

- Collect a much larger set of photographs from LANDSAT 1 and LANDSAT 2 to derive precise quantitative relationships between sun elevation angles, cloud cover, cloud height and cloud shadows. This is of primary importance for elevation angle of less than 30°.

- Analyze additional levels of the stratosphere with existing data to derive more detailed information on the height dependence of stratospheric profiles.

- Derive grid values for the eastern half of the Northern Hemisphere to the extent possible, using stations in that region.

- Compute tropospheric daily variances for the equatorial region from daily grid data and improve the Southern Hemisphere variances using station data and other analyses of that hemisphere.

- Perform a detailed analysis of the 20-25 km region and the 26-30 km region to verify the characteristics of the two data sets and to adjust the analyses as necessary.

- Modify the 4-D simulation programs to curve-fit the newly derived parameters at all levels and to provide interpolation to any latitude and longitude.

The revised 4-D model and the cloud data bank are extremely useful in their current form and there is little question as to the reliability of the data banks. The above suggestions are made simply to further extend the precision of these data banks and to replace certain approximations with measured values.

6. BIBLIOGRAPHY

Barnes, J. C. and D. T. Chang, 1968: Accurate Cloud Cover Determination and Its Effects on Albedo Computations, Final Report Contract No. NAS5-10478, Allied Research Associates, Concord, Mass. 01742

Belmont, A. D., D. G. Dartt and G. B. Nastrom, 1975: "Variations of Stratospheric Zonal Winds, 20-65 km, 1961-1971," Journal of Applied Meteorology, 14(4), pp. 585-594.

Chang, D. T. and M. G. Fowler, 1973: Use of 4-D Atmospheric Models in Simulation of Radiometric Measurements, NASA CR-129007.

Chang, D. T. and J. H. Willand, 1972: Further Developments in Cloud Statistics for Computer Simulations, NASA CR-61389.

Chang, D. T. and J. H. Willand, and M. G. Fowler, 1973: Study of Conditionality and Other Factors Affecting the Use of Cloud Type Statistics in Simulation, Interim Report, Contract No. NAS 8-28721, Environmental Research & Technology, Inc., Lexington, Mass.

Components of the 1000-mb Winds (or Surface Winds) of the Northern Hemisphere, 1966: The Chief of Naval Operations, NAVAIR 50-1C-51.

Crutcher, H. L. and J. M. Meserve, 1970: Selected Level Heights, Temperatures and Dew Points for the Northern Hemisphere, Commander Naval Weather Service Command, Navair 50-1C-52.

Fowler, M. G., J. H. Willand, D. T. Chang and J. L. Cogan, 1974: Studies in the Use of Cloud Type Statistics in Mission Simulation, Final Report, Contract No. NAS8-28721, Environmental Research & Technology, Lexington, Mass.

Greaves, J. R., D. B. Spiegler and J. H. Willand, 1971: Development of a Global Model for Simulating Earth-Viewing Space Missions, Final Report Contract NAS 8-25812, Allied Research Associates, Inc. (NASA CR-61345).

Groves, G. V., 1971: Atmospheric Structure and Its Variations in the Region From 25 to 120 Km, Environmental Research Papers, No. 368, AFCRL-71-0410.

Heastie, H. and P. M. Stephenson, 1960: Upper Winds Over the World; Parts I and II, Her Majesty's Stationery Office, London.

High Altitude Meteorological Data, 1971: World Data Center A, Meteorology Data Report, U.S. Department of Commerce NOAA, N. C., Vol. 3-8.

High Altitude Meteorological Data, 1973: World Data Center A, Meteorology Data Report, International Delayed Data Issue, U.S. Department of Commerce, NOAA, N. C., Vol. 1-5.

6. BIBLIOGRAPHY (Continued)

Justus, C. B., R. G. Roper, and A. Woodrum, 1974: A Global Scale Engineer-
ing Atmospheric Model for Surface to Orbital Altitudes, prepared
for NASA George C. Marshall Space Flight Center, Marshall Space
Flight Center, Alabama.

Lahey, J. F., R. A. Bryson, E. W. Wahl, L. H. Horn, and V. D. Henderson,
1958: Atlas of 500 mb Wind Characteristics for the North..rn
Hemisphere, The University of Wisconsin Press, Madison.

Newell, R. E., J. W. Kidson, D. G. Vincent and G. J. Boer, 1972:
The General Circulation of the Tropical Atmosphere, M.I.T.,
Cambridge, Mass.

Oort, A. H. and E. M. Rasmusson, 1971: Atmospheric Circulation Statistics,
U.S. Department of Commerce, Rockville, Md.

Sherr, P. E., A. H. Glaser, J. C. Barnes and J. H. Willand, 1968:
Worldwide Cloud Distribution for Use in Computer Simulations, Final
Report Contract NAS 8-21040, Allied Research Associates, Inc.

Singleton, F. and D. J. Smith, 1960: Quarterly Journal of the Royal
Meteorological Society, 86.

Spiegler, D. B. and M. G. Fowler, 1972: Four-Dimensional Atmospheric
Models (Surface to 25 km Altitude), NASA CR-20820.

Spiegler, D. B. and J. R. Greaves, 1971: Development of Four-Dimensional
Amtospheric Models (Worldwide), NASA CR-61362.

Webb, W. L. [ed], 1964: Stratospheric Circulation, Academic Press,
New York, 22.

Webb, W. L., 1966: Structure of the Stratosphere and Mesophere, Inter-
national Geophysics Series, Volume 9, Academic Press, New York.